Inês Castanheira Curado Coelho Ferreira

Licenciada em Ciências da Engenharia Química e Bioquímica

Carbon dioxide capture using mixed matrix membranes with metal-organic frameworks supporting ionic liquids

Dissertação para obtenção do Grau de Mestre em
Engenharia Química e Bioquímica

Orientador: Doutora Luísa Alexandra Graça Neves, Investigadora Auxiliar, FCT-UNL

Co-orientadores: Doutora Isabel A. A. C. Esteves, Investigadora Auxiliar, FCT-UNL

Doutor Luís M. Cunha Silva, Investigador Pós-Doutoramento, FC-UP

Júri:

Presidente: Prof. Doutor Mário Fernando José Eusébio
Arguente(s): Doutora Liliana Sofia Carvalho Tomé
Vogal(ais): Doutora Luísa Alexandra Graça Neves

FACULDADE DE CIÊNCIAS E TECNOLOGIA
UNIVERSIDADE NOVA DE LISBOA

Setembro 2017

Inês Castanheira Curado Coelho Ferreira

Licenciada em Ciências da Engenharia Química e Bioquímica

Carbon dioxide capture using mixed matrix membranes with metal-organic frameworks supporting ionic liquids

Dissertação para obtenção do Grau de Mestre em Engenharia Química e Bioquímica

Orientador: Doutora Luísa Alexandra Graça Neves, Investigadora Auxiliar, FCT-UNL

Co-orientadores: Doutora Isabel A. A. C. Esteves, Investigadora Auxiliar, FCT-UNL

Doutor Luís M. Cunha Silva, Investigador Pós-Doutoramento, FC-UP

Júri:

Presidente: Prof. Doutor Mário Fernando José Eusébio
Arguente(s): Doutora Liliana Sofia Carvalho Tomé
Vogal(ais): Doutora Luísa Alexandra Graça Neves

Setembro 2017

Carbon dioxide capture using mixed matrix membranes with metal-organic frameworks supporting ionic liquids

Agradecimentos

Chegado ao final de uma das etapas mais importantes da minha vida, gostaria de agradecer a todas a pessoas que fizeram parte dela e que de alguma forma fizeram com que estes últimos 5 anos se passassem da melhor forma possível.

Um especial agradecimento às Doutoras Luísa Neves e Isabel Esteves e ao Doutor Luís Silva pela oportunidade de participar neste projeto, bem como por toda a ajuda e motivação que me deram ao longo desta etapa.

À doutora Isabel Nogueira do Instituto Superior Técnico pela sua simpatia, entusiasmo, disponibilidade na realização dos testes e esclarecimento de dúvidas momentâneas.

Ao Professor Vítor Alves do Instituto Superior de Agronomia pela disponibilidade na realização dos testes bem como no esclarecimento de qualquer dúvida.

Ao Doutor Rui Ribeiro por se mostrar sempre disponível para ajudar a resolver qualquer problema e a esclarecer dúvidas que foram surgindo, bem como por todas as sugestões dadas.

Ao André Portela por me ter acompanhado nas primeiras semanas, estando sempre disponível para me ajudar e resolver qualquer problema ou dúvida que surgisse.

À Carla Martins e à Carla Daniel por toda a ajuda, esclarecimento de dúvidas e sugestões dadas ao longo destes meses.

Aos meus colegas Gonçalo Marcelo, Gonçalo Martins e Rita Nabais por toda a amizade e ajuda que me deram ao longo desta etapa.

À minha melhor amiga Ana Patrícia Martins por todo o apoio, ajuda e paciência, especialmente durante estes últimos meses, que me ajudou em muito a ultrapassar todos os desafios que ocorreram nesta etapa.

Aos meus pais, à minha tia Fátima e ao meu tio Pedro pelo apoio incondicional e toda a motivação que me deram ao longo destes 5 anos, fazendo com que esta etapa da minha vida decorresse da melhor forma possível.

A todos um grande OBRIGADO!

Resumo

O objetivo desta tese consistiu no desenvolvimento de novas membranas de matriz mista (MMMs) para a captura de dióxido de carbono (CO_2) presente em correntes de pós-combustão.

Neste trabalho foram estudados vários materiais baseados em redes metal-orgânico (MOFs), nomeadamente o MOF MIL-101(Cr) e dois materiais compósitos do tipo IL@MOF, resultantes da incorporação de dois líquidos iónicos (ILs) no MIL-101(Cr), [PMIM][Br]@MIL-101(Cr) e [BMIM][Br]@MIL-101(Cr). Todos estes materiais foram caracterizados estruturalmente, e as suas propriedades texturais e a capacidade de adsorção de CO_2 e N_2 foram também avaliadas.

O equilíbrio de adsorção foi medido numa unidade gravimétrica, numa gama de pressões entre os 0 e os 10 bar à temperatura de 30ºC. Das medições verificou-se que a quantidade adsorvida de CO_2 é superior à de N_2 devido à sua maior afinidade com os adsorventes.

As MMMs preparadas podem dividir-se em três grupos Matrimid®5218/MIL-101(Cr), Matimid®5218/[PMIM][Br]@MIL-101(Cr) e Matrimid®5218/[BMIM][Br]@MIL-101(Cr). Em cada grupo foi utilizada uma matriz polimérica, Matrimid®5218, com diferentes concentrações de enchimento (10%, 20% e 30% (p/p)).

As membranas foram caracterizadas recorrendo a Microscopia Eletrónica de Varrimento (SEM) para avaliar a sua morfologia; Espectroscopia de raios-X por dispersão em energia (EDS) de modo a observar a dispersão do enchimento na matriz polimérica; ensaios de perfuração para avaliar a sua resistência mecânica; ângulos de contacto para determinar a sua hidrofilicidade; Termogravimetria (TGA) para avaliar a sua estabilidade térmica a altas temperaturas e ensaios de permeação gasosa com N_2 e CO_2, a 30ºC.

Os resultados obtidos mostraram que as membranas possuíam uma estrutura densa, existindo uma boa interação entre o polímero, o MOF ou os materiais compósitos IL@MOF. Verificou-se também que a incorporação de MOF nas membranas as torna menos resistentes e que ao adicionar o líquido iónico estas apresentam-se mais resistentes e flexíveis, bem como que a incorporação do MOF ou IL@MOF na matriz polimérica torna as membranas mais hidrofílicas. A analise termogravimétrica demonstrou que todas membranas eram estáveis até 300ºC. Os resultados de permeação gasosa mostraram que a variação da percentagem de incorporação do MOF ou IL@MOF na matriz polimérica influencia o aumento da seletividade CO_2/N_2.

Palavras-Chave: Captura de CO_2, Matrimid®5218, Redes Metal-Orgânico, Líquidos Iónicos, Membranas de Matriz Mista, Adsorção, Permeação.

Abstract

The aim of this thesis was the development of new mixed matrix membranes (MMMs) for carbon dioxide (CO_2) capture from post-combustion flue gas streams.

The synthetized pristine MOF MIL-101(Cr) and new IL@MOF systems, produced by the incorporation of two ionic liquids in MIL-101(Cr), [PMIM][Br]@MIL-101(Cr) and [BMIM][Br]@MIL-101(Cr) were characterized. The textural properties and adsorption capacity for CO_2 and N_2 on these materials were also studied.

The adsorption equilibria of the pure gases N_2 and CO_2 on the mentioned materials were performed by using the gravimetric method in a range of pressures from 0 to 10 bar and at 30ºC. All materials adsorbed higher amounts of CO_2 than N_2, due to the CO_2 higher affinity with the adsorbents.

The prepared MMMs are separated in three groups, Matrimid®5218/MIL-101(Cr), Matrimid®5218/[PMIM][Br]@MIL-101(Cr), Matrimid®5218/[BMIM][Br]@MIL-101(Cr). Each membrane group was prepared using a polymeric material Matrimid®5218 with different concentrations of filler (10%, 20% and 30% (w/w)).

All the prepared membranes were characterized by scanning electron microscopy (SEM), to evaluate their morphology; energy-dispersive x-ray spectroscopy (EDS), to observe the filler dispersion in the polymeric matrix; contact angles to determine their hydrophilicity; mechanical properties to evaluate their mechanical resistance and flexibility; thermogravimetric analysis (TGA) to evaluate their thermal stability and gas permeation experiments with pure gases (N_2 and CO_2) at 30ºC.

The obtained results showed that all membranes have a dense structure exhibiting a good interaction between the polymer, MOF and IL@MOF. It was also verified that with the addition of MOF the membranes turned more fragile, while with the addition of the ionic liquid in the MOF porous structure led to more flexible and resistant membranes. Additionally, it was found that the addition of MOF or IL@MOF in the polymeric matrix turn the membranes more hydrophilic. Thermogravimetric analysis (TGA) showed that all membranes are stable up to 300ºC. Gas permeation results showed that depending on the MOF or IL@MOF concentration on the polymer matrix an increase in CO_2/N_2 ideal selectivity is observed.

Keywords: CO_2 capture, Matrimid®5218, Metal-Organic Frameworks, Ionic Liquids, Mixed Matrix Membranes, Adsorption, Permeation.

Index

Figure Index

Table Index

List of Abbreviations

Abbreviation	
BET	Brunauer-Emmett-Teller
[BMIM][Br]	1-butyl-3-methylimidazolium bromide
EDS	Energy-Dispersive X-Ray Spectroscopy
FEG	Field Emission Gun
FTIR	Fourier-Transform Infrared Spectroscopy
GHG	Greenhouse gas
IL	Ionic Liquid
IPCC	Intergovernmental Panel on Climate Change
IUPAC	International Union of Pure and Applied Chemistry
MIL	Matériaux Institut Lavoisier
MMM	Mixed Matrix Membrane
MOF	Metal Organic Framework
[PMIM][Br]	1-propyl-3-methylimidazolium bromide
PSA	Pressure Swing Adsorption
SEM	Scanning Electron Microscopy
TGA	Thermogravimetric Analysis
TSA	Temperature Swing Adsorption

List of Variables

Variable		Units
F	Force	N
l	Membrane thickness	m
m_s	Mass of the solid	g
m_{sc}	Mass of the measurement cell	g
P	Permeability	$m^2.s^{-1}$
p_{feed}	Feed pressure	bar
$p_{permeate}$	Permeate pressure	bar
q_{net}	Net adsorption amount	
q_{ex}	Excess amount adsorbed	
q_t	Absolute adsorption	
r	Probe radius	m
S	Solubility	
S_c	Cross sectional area	m^2
t	Time	s
V_{Feed}	Feed volume	m^3
V_{Perm}	Permeate volume	m^3
V_A	Average Volume	cm^3
V_p	Pore specific volume	$cm^3.g^{-1}$
V_{sc}	Volume of the measurement cell	cm^3
W	Mass weighted in the balance	g
W_A	Average Weight	g

Greek Letters

Letter		Units
α	Ideal selectivity	
β	Geometric cell parameter	m^{-1}
ρ_s	Solid matrix density	$g.cm^{-3}$
ρ_g	Gas density	$g.cm^{-3}$
σ	Tensile strength	Pa

1. Introduction

Nowadays, due to the rapidly growth of world population and the countries industrialization, energy demand is exponentially increasing.[1] Due to their low-cost, energy density and availability, fossil fuels such as coal, oil and natural gas, are used as primarily source of energy, supporting 85% of the total world demand.[2,3] Fossil fuels have improved human quality life, by allowing the production of a variety of live essential products such as fuels for cars and airplanes, electricity, pharmaceutics and plastics.[4] However, fossil fuels combustion releases high amounts of carbon dioxide (CO_2) into the atmosphere, which is the greenhouse gas (GHG) that most contributes for global warming (more than 60%),[5,3] thus leading to environmental damage and climate changes, such as sea level rising, shrunk of glaciers and very intense heat waves, endangering human life as well as various ecosystems.[6]

Greenhouse effect is very important for life sustainability, because it absorbs the thermal radiation that comes from earth, maintaining suitable temperatures for living; without it would be impossible for any form of life to live on Earth. However, in the last years, GHG concentrations in the atmosphere have increased drastically, especially the CO_2 concentrations. In the past, this GHG was removed naturally, via photosynthesis, but nowadays plants by themselves are no longer capable of remove all CO_2 released to the atmosphere.[7] Since Industrial Revolution, CO_2 concentrations have been exponentially raising, from 280 ppm to nearly 407 ppm in July 2017 [8], corresponding to a raise of about 45%, being 2016 considered the warmest year since 1880.[9] Cumulative anthropogenic CO_2 emissions to the atmospheric system reached 2040 ± 310 $GtCO_2$ between 1750 and 2011 and half of those emissions occurred in the last 40 years, mainly between 2000 and 2010. According the available data, globally in 2014, the energy sector was the main responsible for anthropogenic GHGs release (about 68%), in which 90% corresponded to CO_2 from fossil fuel combustion. Also, in 2014 electricity and heat generation contributed about 42% for fossil fuel combustion, followed by the transport sector (23%) and industry sector (19%).[10]

Currently, about 2.4 million pounds of CO_2 per second are being released into the atmosphere [9] and if the GHGs release rates continuing the same, by 2050 CO_2 atmospheric concentrations may reach about 500 ppm.[3] Due to this critical situation, it became top priority to reduce CO_2 emissions. The Intergovernmental Panel on Climate Change (IPCC), in their latest report (5th Assessment Report) concluded that to avoid the worst scenario of climate change effects it was necessary to keep temperature from rising more than 2ºC compared to the industrial times and that CO_2 emissions should decrease from 41-72% and from 78-118% by 2050 and 2100, respectively, comparing to the 2010 levels.[11] Thus, in December 2015 at the Paris Climate conference (COP21), 195 countries make the first global climate deal in order to reduce the global CO_2 emissions, by following the national climate action plans (INDCs). However, this agreement by itself is not enough to keep global warming below the target of 2ºC.[12] Therefore, carbon capture

and storage (CCS) strategies were developed, which have been considered the best technique to reduce CO_2 emissions.[13] According to the IPCC, CO_2 released in power plants can be decreased by 80-90% if they possess a suitable carbon capture and store process.[14] Carbon capture and storage is a technique composed mainly by three stages, namely CO_2 capture, transport and storage.[15] CO_2 capture phase is the most expensive step (about 75-80% of the total cost), mainly due to the separation of CO_2 from other gases. Thus, it is highly important to find processes with lower cost and high separation efficiency.[15] For CO_2 transportation, the most common via is by pipelines, but it can also be transported by truck and rail (for small quantities) or by ship.[16] Currently, CO_2 is mainly stored in geological formations because of their capacity and environmental properties for the storage at a gigatonne scale, typically consisting in sedimentary basins that include depleting oil and gas reservoirs and saltwater-filled rocks.[17]

For carbon capture three main methods can be applied namely, post-combustion, pre-combustion and oxyfuel combustion, as described in **Figure 1.1**.[18]

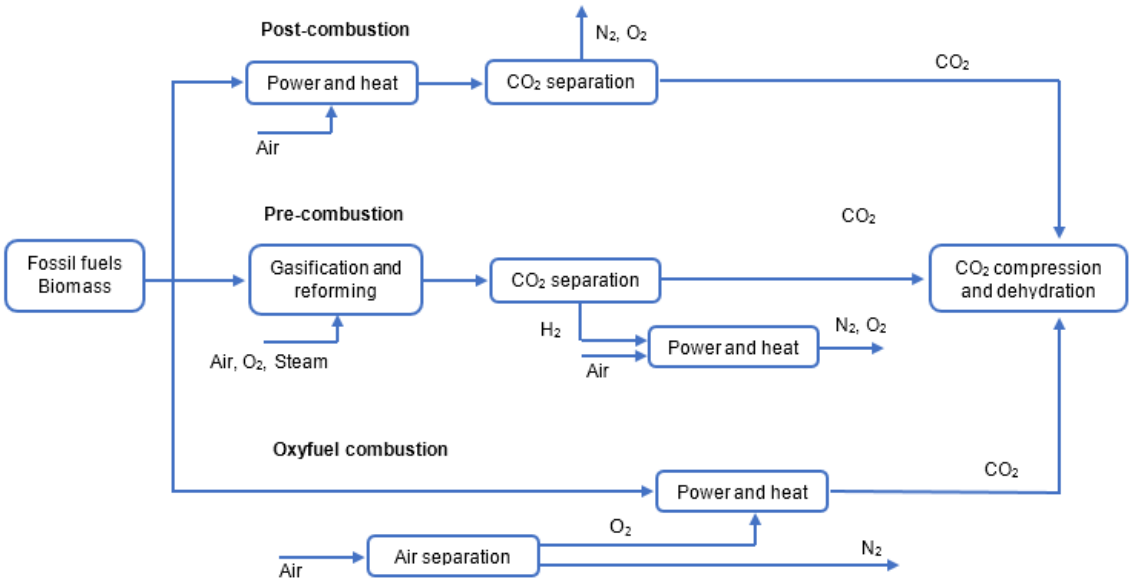

Figure 1.1 – CO_2 capture processes schematic (adapted from [21]).

Post-combustion

Post-combustion processes capture CO_2 from flue gases streams that are produced by burning fossil fuels or biomass. This type of process is mainly used in combustion-based power plants, namely in coal-fired power plants. The fuel is burned with air to produce steam, which drives into a turbine, generating electricity. From this process, a flue stream composed by N_2 from air, water vapor and CO_2 from the hydrogen and carbon present in the fuel as well as some impurities from the coal such as, sulfur dioxide and nitrogen oxides, is obtained.[19] One of the biggest challenges in CO_2 separation from flue gas streams is that it is presented in dilute concentrations (between 2-15vol%, depending on the gas stream) and at low pressures (about 1 bar). Thus, presently the most used method is the absorption by solvent scrubbing using amines

as solvents. Usually, monoethanolamine (MEA) is used, due to its efficiency for low CO_2 partial pressures.[20] In this process, about 85-90% of CO_2 is captured from the flue stream and the CO_2-laden solvent is then regenerated by heat. The captured CO_2 is compressed and then stored.[19]

The post-combustion capture system is currently installed in oil, coal and natural gas power plants, as well as in supercritical pulverized coal fired plants and in natural gas combined cycle plants (NGCC).[19]

Pre-combustion

Pre-combustion processes captures CO_2 from synthesis gas (syngas) streams after the conversion of CO into CO_2. This process consists in the reaction of a fuel with air, oxygen or steam, which origins a stream composed mainly by CO and H_2 (synthesis gas), then the carbon monoxide reacts with steam in a shift converter, producing CO_2 and H_2. The concentration of CO_2 in the stream of CO_2/H_2 at the separation stage is about 15-60vol% with a pressure of 2-7 bar, being separated normally by physical or chemical absorption. Also, a hydrogen-rich fuel stream is obtained, that can be used in a variety of applications such as boilers, furnaces, gas turbines and fuel cells.[21] This type of process is mainly used in oil and coal based integrated gasification combined cycle (IGCC) plants.[19]

The CO_2 capture ratio in pre-combustion processes is 85%, resulting from the conversion ratio of CO into CO_2 (about 90%) and the CO_2 separation efficiency (about 95%), which is similar to the capture ratio in the post-combustion processes. [18]

Oxy-fuel combustion process

In oxy-fuel combustion, nearly pure oxygen (up to 97% purity) is used instead of air in the combustion process, resulting in a flue gas stream composed mainly by CO_2 and H_2O. Since almost pure oxygen is used, process temperatures are very high, so in order to control the temperature, part of the exhaust gases are recycled into the boiler. The flow of CO_2 that is not recycled into the process still contains water vapor and other impurities, namely NO_x and SO_x. Thus, the existing water is condensed, resulting in a purified CO_2 (99% purity) stream, that is ready to be transported and stored. [18]

The advantage of this process is that the partial pressure of CO_2 in the exhaust gases is higher than in post-combustion and pre-combustion processes, which avoids their dilution with N_2 in air. [18] This process can be applied in the same type of power plants as post-combustion capture process.[19]

CO_2 separation methods

All three capture methods previously described have a CO_2 separation step, in which the CO_2 is separated from the other gases present in the flue gas stream. This separation can be done through four distinct methods, such as absorption, adsorption, cryogenic distillation and membrane technology.[15]

Absorption

Absorption is the most used technique, in chemical and petroleum industries, for CO_2 separation, being divided into two types, namely physical absorption and chemical absorption.[1]

- **Physical absorption**

Physical absorption is based on Henry's Law, consisting in the CO_2 capture by a solvent, such as, Selexol™ and Rectisol®. CO_2 is then regenerated by the appliance of heat or pressure reduce. This type of absorption occurs at high CO_2 partial pressures, thus is not very economical when applied to flue gas streams, where the CO_2 partial pressures are commonly lower than 15vol%.[15]

- **Chemical absorption**

Chemical absorption by amine scrubbing is the most widely used technique in the industry for CO_2 separation. In this process, aqueous amine solutions (normally primary amines) are used for the CO_2 absorption, usually monoethanolamine (MEA), which possess a high CO_2 separation efficiency (>90%). Through a zwitterion mechanism the CO_2 reacts with the amine, being then separated in stripping tower by the appliance of heat. The solvent is regenerated being submitted to high temperatures (100-140ºC) at pressures near to atmospheric.[14] However, this process has some drawbacks, because when the CO_2 reacts with the amine solution occurs the formation of carbamates that are associated to a high heat formation, which can cause the degradation of the amine, resulting in solvent loss and equipment corrosion. [11,15] Also the high energy costs relative to CO_2 separation from the amine solution was a decisive factor to develop other methods for CO_2 separation from post-combustion flue gases. [22]

Cryogenic distillation

Cryogenic distillation is a technique that consists on cooling and condensation. This technique is theoretically very attractive for CO_2 separation, although it possesses high energy costs due to the refrigeration requirements. Therefore, this method is only efficient when applied to streams with high CO_2 concentrations, being normally used for CO_2 capture in oxyfuel combustion processes. [11,15]

Adsorption

Since antiquity that adsorption is used by various societies for many applications such as, water desalination, oil and fat clarification and in the treatment of various diseases. However, it was only in the eighteenth century that adsorption ability by porous solids was recognised, being the first quantitative experiments made by Carl Wilhelm Scheele in 1773. After that, adsorption processes have gain more and more importance, mainly in the area of separation technology, industrial catalysis and pollution control. Therefore, over the past years a high demand occurred in discovering new adsorbents and catalysts, new procedures for adsorption data interpretation, namely for micropore and mesopore size analysis, as well as new and more efficient adsorption-based processes. [23,24]

The adsorption phenomenon is defined as the sticking of gas or liquids molecules (adsorbate) to the solid surface of a certain material (adsorbent) (**Figure 1.2**).[23,25] When the adsorbed molecules return to the gas phase it is named desorption, being the inverse process of adsorption.[25] Adsorption phenomenon allows the determination of the solid material capacity to retain a certain adsorbate, by the analysis of the adsorption equilibrium, which is given by the equilibrium between the number of adsorbed molecules and the number of desorbed ones.[23,25] This analysis can be very complex, for example in the case of gas molecules they can present different sizes, structures and electric properties, as well as the solid surface which can have different sites for adsorption. [25]

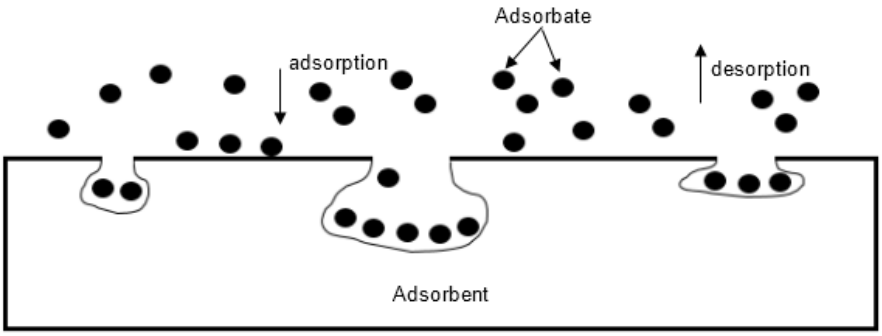

Figure 1.2 – Schematic of adsorption and desorption procesess (adapted from[25]).

The adsorption phenomenon consists in the interaction between a solid surface and gas or liquid molecules. Thus, depending on the interaction energy, two types of adsorption can be distinguished, namely, physisorption and chemisorption.[25]

- **Physisorption**

In physisorption systems the adsorbed molecules do not react with the solid surface, being weakly bounded to it, normally by Van der Waals or induced dipole-dipole interactions.[25] Also, the adsorbed molecules preserve their identity, since upon desorption they return to their

original form. Furthermore, this phenomenon is always exothermic and at high pressures generally occurs as a multilayer. [23,25]

- **Chemisorption**

In chemisorption systems, the adsorbed molecules are strongly connected to reactive parts of the solid surface, being this process restricted to a monolayer.[23,25] Normally, an activation energy is necessary and at low temperatures sometimes the thermal energy is not enough to reach the thermodynamic equilibrium. Also the adsorbed molecules cannot be reversible desorbed from the sorbent.[23]

From the above described adsorption types, physisorption is the process where the adsorbed molecules can be reversible desorbed, so through this type of adsorption is possible to determine the capacity of a certain adsorbent. One way of having a visual analysis of the amount adsorbed is through adsorption isotherms, which reproduce the relation between the amount adsorbed of a certain component by unit mass of adsorbent solid and the equilibrium pressure (or concentration), at a constant know temperature.[26]

Physisorption isotherms are divided into six principles types, according to the International Union of Pure and Applied Chemistry (IUPAC) 1985 more recent classification. This six groups are classified by Types I(a), I(b), II, III, IV(a), IV(b), V and VI (**Figure 1.3**). [27]

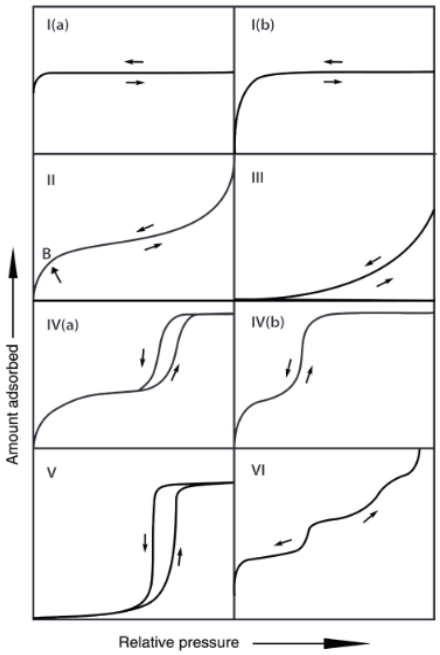

Figure 1.3 - IUPAC six types of isotherms. [27]

- **Type I**

Isotherms type I are usually reversible and obtained by microporous solids with a small external surface such as, some activated carbons or molecular sieve zeolites. Also, this type of isotherms exhibits a limiting uptake, that is principally defined by the accessible micropore volume. Furthermore, type I isotherms are divided in two sub-types: type I(a) and type I(b). Type I(a) corresponds to microporous materials, which possess mainly narrow micropores (width< 1nm) and type I(b) is for materials with a higher range of pore size distribution, that includes wider micropores and some narrow mesopores (width <2.5nm). [23,27]

- **Type II**

This type is usually given by most gases when in contact with nonporous or macroporous adsorbents, being normally characterized by a monolayer-multilayer adsorption up to high relative pressures.[23] When the monolayer is completely covered the isotherm presents a more sharp knee and point B (**Figure 1.3**) indicates when the coverage of the monolayer is completed. If the monolayer coverage presents an excess of amount the multilayer adsorption begins. In this case, the isotherm will present a more gradual curvature and point B will be less distinctive. [23,27]

- **Type III**

In Type III isotherms, the interactions adsorbate-adsorbate are stronger than the adsorbent-adsorbate interactions.[23] Thus, the aggregates of adsorbed molecules are located in the most active areas of the surface. When the pressure is raised the monolayer concentration increases, but before the monolayer complete coverage, a type of co-operative multilayer adsorption occurs, in which molecules are aggregated in the most favourable sites. So, in this type of isotherm it is impossible the appearance of point B and in extreme cases is almost impossible to detect the adsorption, even at high partial pressures.[23,27]

- **Type IV**

This type of isotherms has an initial monolayer-multilayer adsorption like type II isotherms, however it is followed by pore condensation (gas condensation in the pore). Type IV isotherms are characterized by mesoporous adsorbents, in which the adsorption behaviour is controlled by the interactions adsorbent-adsorptive and those between molecules in condensed state. Also, these types of isotherms are separated in two sub-types, one that describes the occurrence of hysteresis effect (IV(a)) and other that describes a completely reversible isotherm (IV(b)). In the case of IV(a), the hysteresis effect occurs when the pore width is exceeded (width >4nm) and depends on the temperature and adsorption system.[23,27]

- **Type V**

Isotherms type V, for the same gas solid-system, are very similar to type III isotherms in the initial section. That is due to the weak bounds between the adsorbate-adsorbent interactions. However, in this case the initial sharp increase depends on the pore size. [23,27]

- **Type VI**

This type of isotherms has a unique shape, which is due to a layer-by-layer adsorption of non-polar molecules on uniform nonporous surface.[23] Each step-height in the isotherms represents the adsorbed layer boundaries, being the capacity given by the inflection points. The sharpness of each step depends on the system and on the temperature.[23,27]

To determine the adsorption capacity of a certain material and obtain the respective isotherms, it is necessary to measure the respective adsorption isotherms. The most common experimental techniques used to measure the adsorption/desorption equilibria are the gravimetric and volumetric methods.

- **Volumetric/Manometric method**

The volumetric method is the oldest technique used for gas adsorption on solid materials.[25] This method consists in the addition of a certain pressure to a reference calibrated volume and posterior expansion of that pressure to a cell that contains the adsorbent. The adsorption process begins when the adsorbate enters in contact with the adsorbent, with a consequent decrease in bulk pressure until the equilibrium is reached. Adsorption equilibrium points are measured with the admission of pressure; when the maximum desired pressure is reached, a stepwise depressurization of the system is made, which gives the respective desorption points.[28] For the construction of the isotherm, the amount adsorbed is calculated by a mass balance given by the difference between the final and initial pressures, and previously knowing the solid mass and both reference and cell volumes. This method as the advantage of being simple, not requiring any high-tech or expensive equipment.[25]

- **Gravimetric method**

Gravimetric method is a more recent than the volumetric method, being used to the characterization of porous media, in gas adsorption equilibria and in the adsorption kinetics investigation.[25]

This method consists in the admission of a certain pressure to a cell containing the adsorbent, however in this case a more precise system is used. In every point of the isotherm the mass is directly measured, by an ultrasensitive and accurate microbalance, which can detect even the slightest mass variation.[29] This method requires a more complex apparatus, having the

consequence of being more expensive than the volumetric method. Also, magnetic suspension balances are highly sensitive to electromagnetic or mechanical interferences and even the electromagnetic fields prevenient from heating systems or other wires in the lab can eventually interfere with the measurements. [25]

In gas adsorption separation, the characteristics of the material used play a very important rule. Therefore, a good material for adsorption should possess a high superficial area combined with a high porous volume. Also, the kinetics of the material should be taken into account, because a solid with a good capacity but a very slow kinetic it is not a very good material, since it would take a long time before the adsorbate molecules could reach the particle interior and vice-versa.[30]

The well-known adsorbents used in gas separation by adsorption processes are molecular sieves, activated carbon, zeolites, calcium oxides, hydrotalcites and lithium zirconate.[11] However, in the past decade metal organic frameworks (MOFs) due to their high surface area, tunable pore size and high micropore volume, have gained special interest has good candidates for gas storage, especially for N_2, CH_4 and CO_2.[31]

For carbon dioxide separation from flue gas streams the adsorption techniques that are commonly used are pressure swing adsorption (PSA) and temperature swing adsorption (TSA), being the differences between them relying on the adsorbent regeneration strategy.[32]

- **Pressure Swing Adsorption (PSA)**

PSA is a cyclic process, where the CO_2 is adsorbed from the post-combustion flue gas stream by passing through an adsorbent bed, at high pressures. Then, before the adsorbent bed gets saturated, a regeneration is carried out, where the CO_2 is removed by reducing the total pressure.[33,34] This process can have efficiencies higher than 95%, being an available technology for CO_2 capture from power plants.[11]

- **Temperature Swing Adsorption (TSA)**

In this method, the regeneration of the adsorbent is carried out with the increase of bed temperature, normally by the injection of hot air or steam, at a constant pressure.[32] The obtained CO_2 has a purity higher than 95%, although the regeneration time is longer than in PSA process.[11]

Membrane technology

Membrane separation processes consists in using membranes as a permselective barrier, that transports more easily one component of the feed mixture than the others (**Figure 1.4**). This phenomenon occurs due to the different physical and chemical properties of the membrane material and the permeating components. [35,36] Membrane based separation has come

up as a promising process to a variety of industrial processes, such as in the separation of CO_2 from flue gas, natural gas and syngas [37] as well as hydrogen isolation and recovery, oxygen enrichment from air and nitrogen enrichment from air.[38,39]

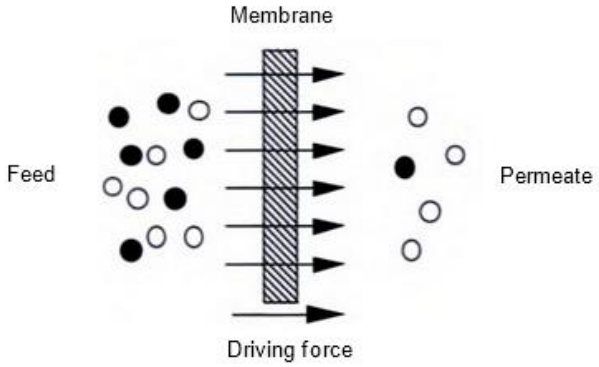

Figure 1.4 – Schematic of membrane separation process. [36]

Membrane technology systems are very attractive for CO_2 capture processes due to its intrinsic advantages such as high energy efficiency (saving up to 50% of energy[38]), simplicity in the operational equipment as well as a small footprint and relatively easiness in the scale up.[37] Also, one of the most important properties of membranes consists on the ability to control the permeation rates of different species. The types of membranes used in gas separation processes are divided in three groups: polymeric membranes, inorganic membranes and mixed matrix membranes.[37,39]

- **Polymeric Membranes**

Due to their low-cost, easy manufacture and mechanical flexibility, polymeric membranes are the type of membranes most commonly used in industry. When using dense polymeric membranes, the gas permeation is controlled by the mechanism of solution-diffusion, in which the permeability of a gas is given by the relation between its diffusion and solubility coefficient in the membrane.[40] The most common type of polymers used in gas separation are polyimide, polysulfone, cellulose acetate, silicon rubber and polyphenylene oxide.[43] However, these type of membranes possess low thermal and chemical stabilities as well as a trade-off between selectivity and permeability, which means that higher selectivities traduces into a lower permeabilities and high permeabilities into low selectivities.[41,42]

The trade-off concept between permeability and selectivity is associated to an upper bound, which was firstly reported in 1991 by Robeson, who upon the analysis of over 300 references about membrane gas separation studies discovered a relationship between permeability and selectivity. This relationship could be graphically represented as a limit (upper bound) by the log of the separation factor versus the log of the higher permeable gas. Robeson upper bound of 1991 was valid for variety of gas pairs excepting for CO_2/N_2 separation because

the data existing at the time did not follow the upper bound protocol. [46] In 2008, new correlations for different gas pairs, including CO_2/N_2 separations were developed (**Figure 1.5**).[47]

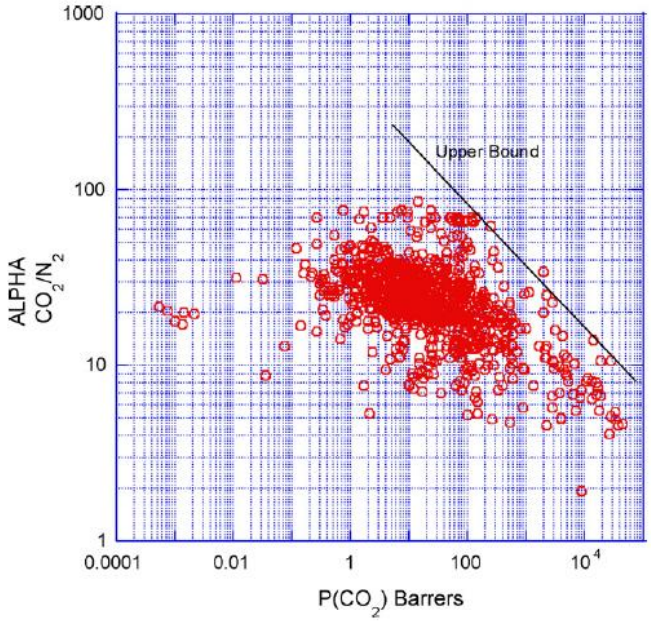

Figure 1.5 – Upper bound correlation for CO_2/N_2 separation. [47]

- **Inorganic Membranes**

Inorganic membranes are divided in four types, namely, ceramic membranes, glass membranes, metallic membranes and zeolitic membranes. Normally, they possess higher chemical and thermal stability than polymeric membranes as well as higher permeabilities and selectivities (especially for activated carbon and zeolites). However, they have low mechanical resistance, low reproducibility on properties as well as a high manufacturing cost when compared with polymeric membranes. These disadvantages represent the main challenges for the use of inorganic membranes at industrial level.[36,43,44]

- **Mixed matrix membranes**

In order to overcome the disadvantages of both polymeric and inorganic membranes mixed matrix membranes were developed. This type of membranes is composed by an inorganic filler (dispersed phase) dispersed in a polymeric matrix (continuous phase).[38] This combination provides to the membranes the mechanical flexibility and easy processability of polymeric materials as well as the high separation performances of inorganic materials, which results in resistant membranes with a good separation performance. [38,44,45]

In MMMs, the properties of both polymer and inorganic filler affect the membrane performance. Regarding the polymeric matrix, glassy polymers with a high selectivity are preferred comparing to high permeable rubbery polymers with low selectivity.[35] As for the

inorganic fillers, their surface and chemical structure as well as particle size distribution are the main properties to be considered, being zeolites, mesoporous silicas, activated carbons, carbon nanotubes and non-porous solids commonly used.[48] However, due to the manufacture of successful mixed matrix membranes, the polymer-filler interactions need to be strong and these materials have shown low compatibilities towards the polymeric matrix. Some of the them presented non-ideal structures such as rigid polymeric layer, particle pore blockage and formation of non-selective voids in the membrane matrix, which affects the membrane separation performance. [35,45,49]

Therefore, the discovery of new materials with a high affinity to the polymer matrix turned crucial for the development of mixed matrix membranes. Materials such as, metal organic frameworks (MOFs) due to their properties, have gained interest as inorganic fillers for mixed matrix membranes.[43]

Metal organic frameworks (MOFs) are a new group of hybrid porous materials which have been developed in the last decade. They are constituted by inorganic metal centres and organic linkers which are connected through coordinated bonds. This new group of materials have gained interest in a wide range of applications, namely for gas separation and storage, catalysis, drug delivery, sensor technology and microelectronics, due to its unique characteristics. MOFs usually possess high surface areas (>6000 m^2/g), high porosities and good thermal and mechanical stability. However, the property that make these materials more interesting is that by changing the combination of their organic linkers and metal complexes it is possible to enhance their affinity towards different gases, which can result in higher permeabilities and selectivities.[41,43] Moreover, due to their organic nature, higher pore volume and low density, they have shown a better compatibility with the polymer than the common inorganic fillers, which helps to avoid the formation of the "sieve-in-cage" morphology (existence of gaps between both phases).[48,50] Previous works using mixed matrix membranes with MOFs as inorganic fillers have shown an increase of both selectivity and permeability when compared with the results using only the polymeric membrane. Dorosti *et al*. studied the separation performance of Matrimid/MIL-53 mixed matrix membranes and observed a 94% increase in permeability as well as a 84% increase in CO_2/CH_4 selectivity when compared with pure Matrimid membranes, for a 15wt% MOF loading. [49]. The studies of Perez *et al*. showed similar results in which Matrimid/MOF-5 MMMs were prepared being observed at 30wt% MOF loading an increase of 120% in the permeability, although in this case the selectivities remained constant.[44] However, the incorporation of MOFs in the polymeric matrix may turn the membranes more fragile and rigid. In previous works, one of the used strategies to overcome this problem was the incorporation of ionic liquids in the MOF porous structure (IL@MOFs)[51].

Ionic Liquids (ILs) are molten salts constituted by organic cations and inorganic or organic anions, which are in the liquid state at room temperature. This characteristic is explained by the low intermolecular interactions, low packing of their asymmetrical ions and also their charges

delocalization, which lead to low melting temperatures. [52,53] These materials also possess other interesting properties such as, nonflammability, negligible volatility, high ionic conductivity and high chemical and thermal stability. But, the characteristic that made them very promising materials is the fact that their physical and chemical properties can be tuned only by changing the cation or anion in their structure. Due to all these properties, ionic liquids are considered novel "green" solvents with a very promising future in many applications, such as chemical reactions, extractions, catalysis and gas separation. [52,54] In this last one, ionic liquids have been most successful in CO_2 capture/separation, due to the interactions between the molecules of the CO_2 quadrupole moment and the ILs electric charges.[53]

Ionothermal synthesis was the first method for ILs incorporation in MOFs, however more recently post impregnation strategies to prepare the IL@MOFs have been reported, in which the ILs are incorporated in the MOFs after the synthesis of the MOF. Three main strategies of post impregnation have been studied, in which the first consists in mixing a solution of ILs with the MOF powder with the help of a solvent. This method is the most used for the impregnation of the ionic liquids in MOFs that possess coordinatively unsaturated sites. The second strategy is called ship-in-bottle where the ionic liquid is synthetized within the porous of the MOFs. In the last strategy, the ionic liquids are introduced in the MOF porous structure through capillary action. [52]

The main objective of this thesis was the development and characterization of new mixed matrix membranes with metal organic framework supported ionic liquids for the separation and capture of CO_2 from flue gas streams in post-combustion processes.

In this work MOF MIL-101(Cr) and two new IL@MOF systems, [PMIM][Br]@MIL-101(Cr) and [BMIM][Br]@ML-101(Cr), were used. These materials were characterized by different techniques such as, scanning electron microscopy (SEM), thermogravimetric analysis (TGA), N_2 isotherm at 77K and equilibrium adsorption measurements with N_2 and CO_2 at 30ºC, in order to evaluate their textural properties and adsorption capacity.

For the preparation of the MMMs, Matrimid®5218 was used as polymer, being the prepared membranes divided in three groups, namely Matrimid®5218/MIL-101(Cr), Matrimid®5218/[PMIM][Br]@MIL-101(Cr) and Matrimid®5218/[BMIM][Br]@MIL-101(Cr) membranes.

The prepared MMMs were studied to evaluate if the incorporation of the ionic liquids in the MOFs porous structure enhanced the membrane properties as well as the CO_2/N_2 ideal selectivity and CO_2 permeability when compared with the membranes composed only by the MOF.

All prepared membranes were characterized by different methods: scanning electron microscopy (SEM) to evaluate their morphology; energy-dispersive x-ray spectroscopy (EDS) to

observe the materials dispersion in the polymeric matrix; contact angle to determine their hydrophilicity; mechanical properties to evaluate their resistance and flexibility; thermogravimetric analysis (TGA) to evaluate their thermal stability and gas permeation experiments with pure gases (N_2 and CO_2) at 30ºC.

2. Materials and Methods

2.1 Materials

Mixed matrix membranes (MMMs) were prepared using a polymeric material – Matrimid® 5218 (Hunstman, USA) and chromium(III) terephthalate metal-organic framework (MIL-101(Cr)). Dichloromethane (Sigma Aldrich, >99.9%) was used as solvent. Moreover, two ionic liquids, namely, 1-propyl-3-methylimidazolium bromide ([PMIM][Br]) and 1-butyl-3-methylimidazolium bromide ([BMIM][Br]), were also incorporated within MIL-101(Cr) porous structure to produce two distinct materials to be characterized either as adsorbents or in the MMMs. Both MOF and ionic liquids were synthesized by our collaborators at REQUIMTE Porto, Faculty of Sciences, University of Porto.

Gases N_2 (Praxair, USA) with 99.99% purity, CO_2 (Praxair, USA) with 99.998% purity and Helium (Praxair, Portugal) with 99.999% purity were used in the present work.

Matrimid® 5218

Matrimid® 5218 is a polyimide that is widely used in membranes for gas separation studies.[49] This polyimide possesses high thermal and mechanical stability, being soluble in most common organic solvents, such as dichloromethane (DCM), chloroform and dimethylformamide (DMF).[55,56]

The chemical structure of Matrimid® 5218 is represented in **Figure 2.1**

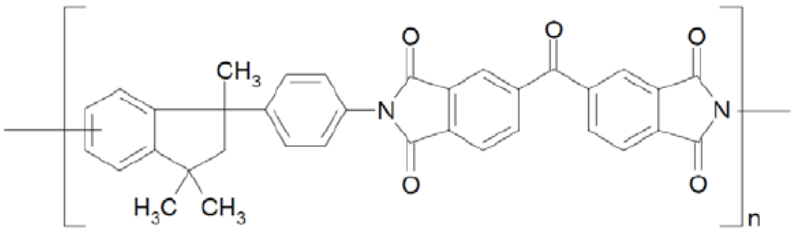

Figure 2.1 – Matrimid® 5218 chemical structure. [56]

Metal Organic Framework MIL-101(Cr)

Chromium(III) terephthalate metal-organic framework (MIL-101(Cr)) is formed by super tetrahedra units (STs) which are composed by trimeric chromium (III) octahedral clusters interconnected with terephthalate linkers (organic linkers).[57] These units are micro porous having windows with free apertures of 8.6 Å, that when connected to each other give origin to a mobil thirty-nine (MTN) type zeolite framework, with two geometric types of windows free apertures: pentagonal (12 Å) and hexagonal (16 Å x 14.7 Å).[31,57] MIL-101(Cr) also possesses two types of

mesoporous cages with 29 Å and 34 Å of diameter (**Figure 2.2**) and a large quantity of active metal unsaturated chromium sites (approximately 3.0 mmol/g), that are capable of capturing CO_2 due to the Lewis acid-base interactions between the O of the CO_2 and Cr(III).[31,58] Furthermore, MIL-101(Cr) is one of the most porous MOFs, having an excellent CO_2 adsorbing capacity (23 mmol/g at 30 bar and 298 K), as well as a high hydrothermal stability, not suffering any changes when submitted to high temperatures in a variety of organic solvents and water.[58,59]

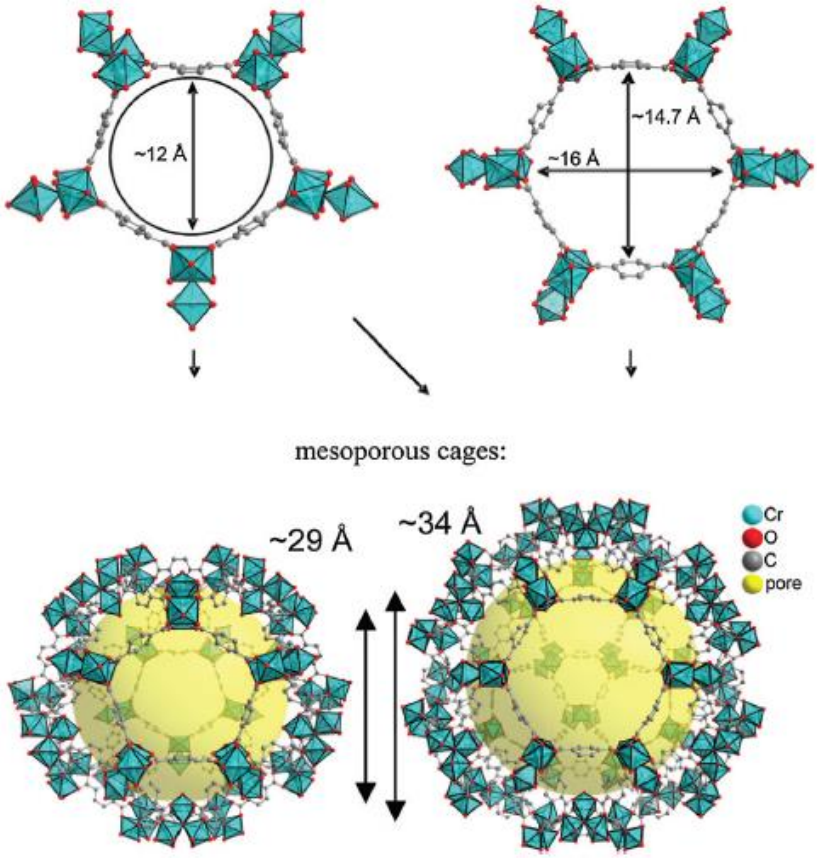

Figure 2.2 – Chemical structure of MOF MIL-101(Cr). [57]

Ionic Liquids

In this work, apart from the pristine MIL-101(Cr), two ionic liquids were incorporated – at REQUIMTE-Porto within the MOF MIL-101(Cr) porous structure, namely, 1-propyl-3-methylimidazolium bromide ([PMIM][Br]) and 1-butyl-3-methylimidazolium bromide ([BMIM][Br]). **Table 2.1** resumes the ionic liquids properties.

Table 2.1 – [PMIM][Br] and [BMIM][Br] chemical properties

Ionic Liquid	Molecular Weight (g/mol)	Viscosity (mPa.s) (25ºC)	Density (g/cm^3) (25ºC)
[PMIM][Br]	205.09 [60]	-	1.32 [61]
[BMIM][Br]	219.12 [62]	363.00 [62]	1.23 [62]

2.2 Methods

2.2.1 MOF and IL@MOFs synthesis

The metal organic framework MIL-101(Cr) synthesis was carried out following the original method described by Férey and co-workers [63] and the ionic liquid 1-Propyl-3-Methylimidazolium ([PMIM][Br]) also by a previous reported protocol [64]. Regarding the IL@MOF materials, [PMIM][Br]@MIL-101(Cr) (here described as ADILS7A and ADILS7B) were synthesized by direct contact method and [BMIM][Br]@MIL-101(Cr) (here described as ADILS8) by the ship-in-bottle method. A detailed description of the materials synthesis is in **Appendix 7.1**.

2.2.2 Adsorption Equilibria

Firstly, the powdered adsorbents MIL-101(Cr), ADILS7A, ADILS7B and ADILS8 were subjected to adsorption equilibria measurements, to test their gas adsorption capacity towards, N_2 and CO_2. All materials were previously degassed at high temperature in order to ensure that the solids are free of impurities and humidity. The adsorption/desorption equilibria studies were done at a controlled temperature of 30ºC (Julabo F32, ±0.1º) in high-precision (0.01mg) ISOSORP 2000 high-pressure magnetic-suspension microbalance (Rubotherm GmbH, Bochum, Germany).[29]

N_2 adsorption isotherm at 77K

This analysis was done to MIL-101(Cr), ADILS7A, ADILS7B and ADILS8 powders, to determine their BET superficial surface area and porous volume. All measurements were done in a ASAP2010 (Micromeritics) equipment. This analysis is required to evaluate if the material has potential to capture and separate gases such as CO_2. Moreover, the results obtained are essential to determine the total adsorbed quantities in the solids.

Helium picnometry

Helium picnometry was used to determine the density of the solid matrix, discarding its porosity. This result is required to calculate the amount adsorbed quantities in the solids. In this analysis, it is assumed that helium acts as a non-adsorbing probe molecule. The density was

measured by a gravimetric method in a ISOSORP 2000 high-pressure magnetic-suspension microbalance (Rubotherm GmbH, Bochum, Germany).[29]

Gravimetric sorption method

For adsorption/desorption isotherms measurements the standard static gravimetric method was used.[29] **Figure 2.3** shows a schematic of the apparatus used, which consists in a high-precision ISOSORP 2000 high-pressure magnetic suspension balance (Rubotherm GmbH, Bochum, Germany), that can measure the weight of two samples at the same time. Also, several pressures transducers were used, in order to have a more precise measure at all pressures. For pressures between 0 and 1 bar an accurate Baratron model 627D (MKS Instruments GmbH, Germany) was used and for 0-10 bar, 0-35 bar and 0-138 bar Omegadyne Inc. pressure transducers were employed, model PX01C1-150A5T, PX01C1-500A5T and PX03C1-3KA5T, respectively. To control the temperature a thermostatic bath F32 HL (Julabo GmbH, Germany) was used. The pressure was monitored and recorded at real time using in-house developed Labview software.

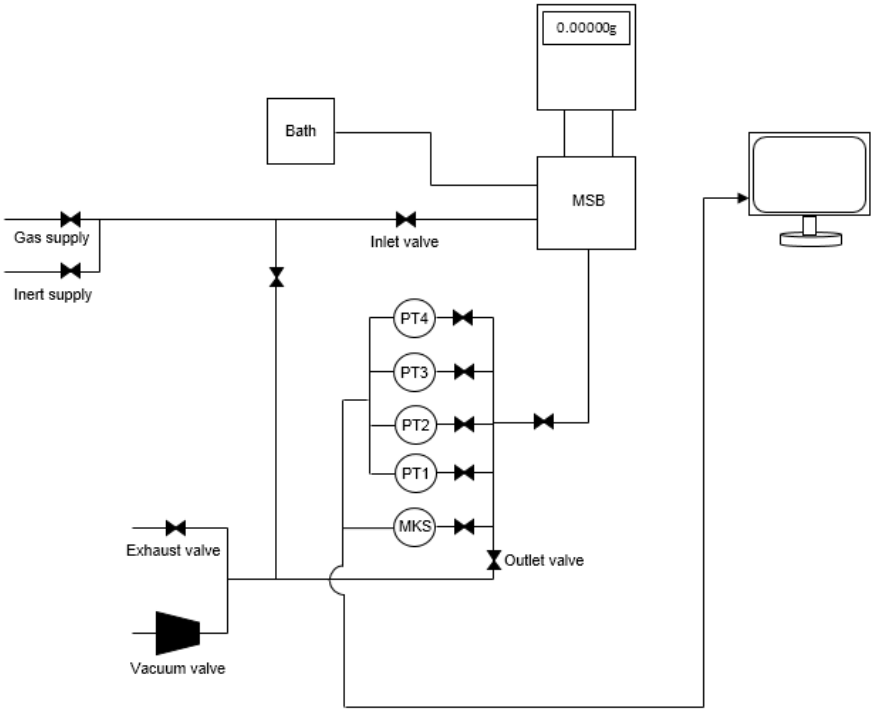

Figure 2.3 – Schematic of gas adsorption apparatus (MSB – Magnetic suspension balance; PT – Omegadyne pressure transduscer; MKS – MKS Baratron transducer).

Adsorption/ Desorption equilibria measurements

Before each isotherm, a degassing of the solid samples is done, to ensure that within the material does not exists any impurities or other adsorbed materials. In this work, the samples were degasified in an oven (Nabertherm B150 GmbH, Germany), with a 2ºC/min heat ramp until reaching 150ºC, staying at this temperature during 3h. The temperature at which the adsorption

cells are degasified is determined based on Thermogravimetric analysis (TGA) analysis results. After this procedure both samples are placed inside the magnetic balance.

Adsorption measurements begins with the admission of a certain pressure into the cells containing the degassed samples, by opening the inlet valve. Then, the pressure and both cells weight changes are monitored until the equilibrium is reached, which is assumed to happen when both variables rate change is near zero. This process is repeated until the maximum desired pressure is reached. A stepwise depressurization is followed, by opening the outlet valve. In this work, a maximum pressure of 10 bar was reached, with 9 points recorded per isotherm.

The samples mass measured are made using a magnetic suspension balance. This balance has three stages: zero point, Measure point 1 (MP1) and Measure point 2 (MP2) (**Figure 2.4**). At zero point stage the magnet is freely suspended and the balance is tared to cancel any weight shifts due to the electronics and be able to measure MP1 and MP2. After the balance is tared, MP1 stage is chosen, where the first (bottom) sample is lifted and its mass measured. Afterwards, MP2 stage is chosen, where the second (upper) sample is lifted up together with the first sample and the mass of both samples is weighted. Thus, the mass of the second sample is obtained by the difference between the mass weighted in MP2 stage and the mass weighted in MP1 stage.

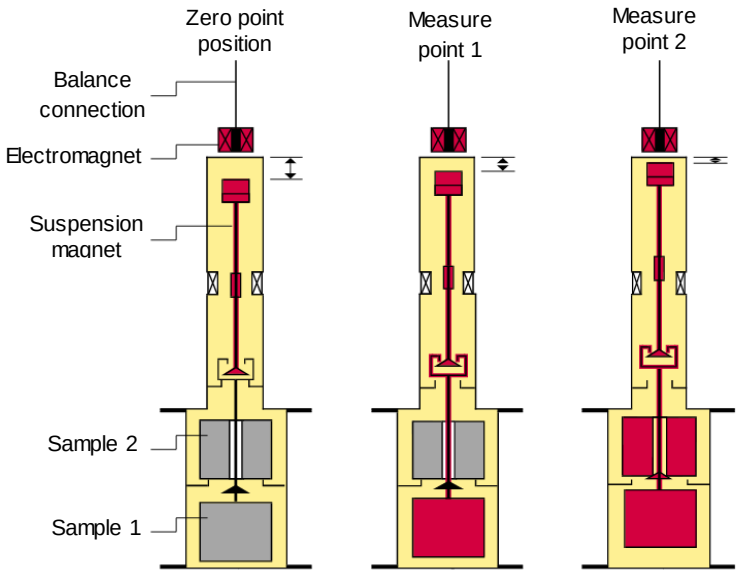

Figure 2.4 - Schematic of magnetic suspension balance three stages. [91]

For the adsorption/desorption equilibrium analysis, three different approaches were used, the first one is the net adsorption (q_{net}), which is given by the amount of adsorbate present within the cell with adsorbent minus the amount of adsorbate present within the same cell without adsorbent, at the same pressure and temperature conditions.[29] Therefore, to calculate q_{net} values **Equation 2.1** was used. [29]

$$q_{net} = \frac{W - m_s - m_{sc} + V_{sc}\rho_g}{m_s} \quad \textbf{(Eq. 2.1)}$$

Where,

W – mass weighted in the balance (g)

m_s – Solid mass within the measurement cell (g)

m_{sc} – Mass of the measurement cell that contributes to buoyancy effects (g)

V_{sc} – Volume of the measurement cell that contributes to buoyancy effects (cm^3)

ρ_g – Gas density at the equilibrium pressure and temperature ($g.cm^{-3}$)

The second approach, is the excess amount adsorbed (q_{ex}), which is represented by the difference between the amount of adsorbate in contact with the adsorbent and the amount of adsorbate that remains in the gaseous phase after the adsorption equilibrium is reached. This parameter is calculated using **Equation 2.2**. [29]

$$q_{ex} = q_{net} + \frac{\rho_g}{\rho_s} \quad \textbf{(Eq. 2.2)}$$

Where,

ρ_s – Solid matrix density ($g.cm^{-3}$)

The last one, is the absolute adsorption (q_t), which represents the total adsorbed amount and is related with both previous approaches [28], being calculated by **Equation 2.3**.[29]

$$q_t = q_{ex} + V_p\rho_g \quad \textbf{(Eq. 2.3)}$$

Where,

V_p – Pore specific volume ($cm^3.g^{-1}$)

The ideal selectivity is given by **Equation 2.4**

$$\alpha_{i/j} = \frac{q_i}{q_j} \quad \textbf{(Eq. 2.4)}$$

Where,

q_i – adsorbed amount of the most retained gas

q_j – adsorbed amount of the least retained gas

For these analyses, the gas densities were taken from NIST Standard Reference Data Base. [65]

2.2.3 Membrane preparation

Matrimid® 5218 membranes

Matrimid®5218 membranes were prepared by solvent evaporation method. Firstly, 0.25g of Matrimid®5218 polymer were dissolved in 2.25 mL of dichloromethane. Then the mixture was submitted to an ultrasonic bath for 4 hours and stirred for 24 hours, on a magnetic stirrer at 600 rpm. Hence, the solution was poured into a Teflon petri dish and placed in a desiccator, in order to provide a slowly solvent evaporation.

Matrimid® 5218/MIL-101(Cr) and Matrimid® 5218/ ADILS8 membranes

A similar protocol was used for the preparation of mixed matrix membranes (MMMs), but in this case different concentrations of MOF MIL-101(Cr) or ADILS8 (10%,20% and 30% w/w) were incorporated in Matrimid®5218. For each membrane, two solutions were prepared, one with 0.25g of Matrimid®5218 and 2.25mL of dichloromethane and other containing the necessary quantity of MOF MIL-101(Cr) or ADILS8, corresponding to 0.025g (10%(w/w)), 0.05g (20%(w/w)) or 0.075g (30%(w/w)), with 2.25mL of dichloromethane. Both solutions were sonicated for 4 hours and stirred for 24 hours. After that, the two solutions were mixed and put to stir for 1 hour. After this period, the solution was poured in a Teflon petri dish and placed in a desiccator.

Matrimid® 5218/ADILS7B membranes

For ADILS7B membranes, the same protocol as for Matrimid®5218/MIL-101(Cr) was used. However, in this case 0.5g of polymer and 4.5mL of dichloromethane were used. Using this method, the membranes with the following percentages of ADILS7B: 10%(w/w), 20% (w/w) and 30%(w/w) which correspond to 0.05g, 0.1g and 0.15g, respectively, were prepared.

2.2.4 Thermogravimetric Analysis (TGA)

In this method, all the solids (MIL-101(Cr) and IL@MIL-101(Cr)) were submitted to a constant raise of temperature until its degradation. The objective is to evaluate the material stability with temperature and analyse the weight loss as a function of the increasing temperature. Moreover, the weight loss can identify the degradation on the main component of the material. All the prepared membranes (Matrimid®5218, Matrimid®5218/MIL-101(Cr), Matrimid®5218/ADILS7B and Matrimid®5218/ADILS8) were also analysed but only until 300ºC.

The powders ADILS7A, ADILS7B and ADILS8 were analysed in a TGA-50 Shimadzu equipment, with a Nitrogen flow rate of 20 $mL.min^{-1}$ and at $2ºC.min^{-1}$ heat rate. MIL-101(Cr) powder and all the membranes were analysed in a Labsys evo TGA-DSC 1600ºC PG system (Seteram, France) at $10ºC.min^{-1}$ heat rate and with an Argon atmosphere.

2.2.5 Scanning Electron Microscopy (SEM)

The prepared mixed matrix membranes as well as the powders of MIL-101(Cr), ADILS7A, ADILS7B and ADILS8 were analysed by scanning electron microscopy (SEM). In the case of the powders analyses, the objective was to determine the particle size and for the membranes was to evaluate if they were suitable for membrane permeation experiments by the analysis of their cross-section and surface, observing if they possess a dense or porous structure.

For the powders analyses, a sample with 10 mg was prepared and in the case of membranes they were broken in 1 cm^2 samples using liquid nitrogen. All samples were covered with a layer of Au-Pd and placed in a SEM device model 240 Hitachi with an electron beam intensity of 20-kV, except for Matrimid®5218+20% MIL-101(Cr) which was analysed in a JOEL FEG-SEM equipment model JSM7001F with an electron beam intensity of 15-kV. All the analyses were made at Instituto Superior Técnico (IST) with the help of Dr. Isabel Nogueira.

2.2.6 Energy-Dispersive X-Ray Spectroscopy (EDS)

Energy-Dispersive X-ray spectroscopy (EDS) technique was used to determine the elements present and its distribution on the membranes prepared. Since all elements have a different atomic structure, the application of a high-energy beam of electrons, protons or X-rays on the sample leads to the appearance of different peaks that are unique to each element. This technique allows elemental identification and quantification as well as elemental distribution (X-ray mapping).

In this work, Matrimid®5218/MIL-101(Cr) membranes surfaces were analysed in a JOEL FEG-SEM equipment model JSM7001F with an Energy Dispersive Spectroscopy (EDS) detector for Oxford light elemental, model INCA 250. This analysis was made to confirm the existence of chromium within the membrane and with the X-ray mapping images, to observe the MIL-101(Cr) distribution in the membrane. Matrimid®5218/ADILS8 membranes surfaces were also analysed, but in this case, to confirm the existence and distribution of bromide (ionic liquid) in the prepared membranes.

2.2.7 Contact Angles

This technique is used to evaluate the hydrophobicity of the prepared membranes through the angle formed between their surface and a drop of water or other solvent. The contact angle of a liquid drop in a solid surface is given by the equilibrium between the drop and three interfacial tensions, namely, solid-vapor (γ_{SV}), solid-liquid (γ_{SL}) and liquid-vapor (γ_{LV}) (**Figure 2.5**). In this analysis to evaluate the hydrophobicity of the prepared membranes water was used. Thus, if the angle is inferior to 90º it means that the membrane is hydrophilic. If the opposite occurs (contact angle superior to 90º) the membrane is considered hydrophobic.

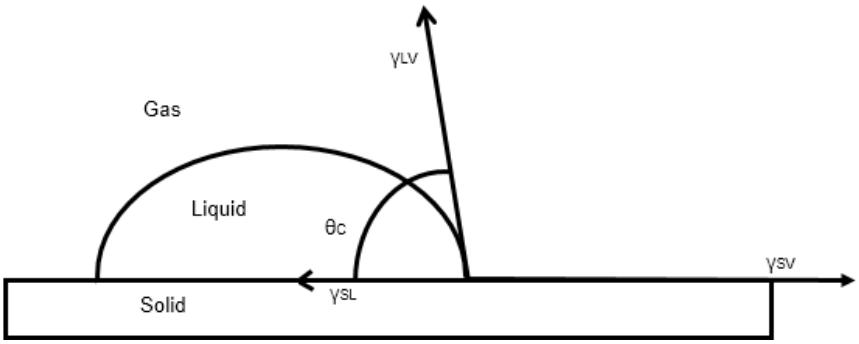

Figure 2.5 – Schematic of all three interfacial tensions.

For contact angles measurements, the software of KSV (CAM2008) was used, that consists on an optic system that captures several images of the drop of water on the membrane surface and calculates the left and right angle made by them. Rectangular shaped membrane samples were used with an undefined dimension and a syringe to put the drop of water in the membrane surface. Furthermore, the software was defined to capture 10 frames in each measure and each sample was measured 3 times, being the final values presented as an average of the 3 measurements.

2.2.8 Mechanical properties

Puncture test measurements were performed to analyse the membrane capacity to resist or transmit an external force without breaking or deform. In all the prepared membranes, the necessary force to puncture them was determined.

All the analyses were performed in Institute Superior de Agronomia (ISA) with the help of Prof. Vitor Alves, using a texturometer analyser (TA XT Plus Texture analyser – Stable Micro Systems, UK). The experiments were done using samples with dimensions of 3x3 cm at room temperature. The apparatus consists in a texturometer analyser with a 2 mm diameter probe, which perforates the sample at a velocity of 1 $mm.s^{-1}$. To register the results and to control the apparatus a software is used, which is also used to calibrate the equipment. Three replicates were done for each sample.

The experiment begins when the probe enters in contact with the membrane, being registered by the software the applied force (N) as a function of time (s) and distance (mm), measured by the probe. The tensile strength (Pa) of each sample was calculated using **Equation 2.5**.

$$\sigma = \frac{F}{S_c} \qquad \textbf{(Eq. 2.5)}$$

Where,

σ – Tensile strength (Pa)

F – Force (N)

S_c – cross sectional area (m^2)

For cross sectional area calculation **Equation 2.6** was used.

$$S_c = \pi \times r^2 \qquad \textbf{(Eq. 2.6)}$$

Where,

r – probe radius (m)

2.2.9 Gas permeation experiments

The main objective of this work was the preparation of mixed matrix membranes for CO_2 separation in post-combustion streams. Thus, gas permeation experiments were made to determinate their permeability and CO_2/N_2 ideal selectivity. For these experiments a gas permeation apparatus shown in **Figure 2.6**, was used.

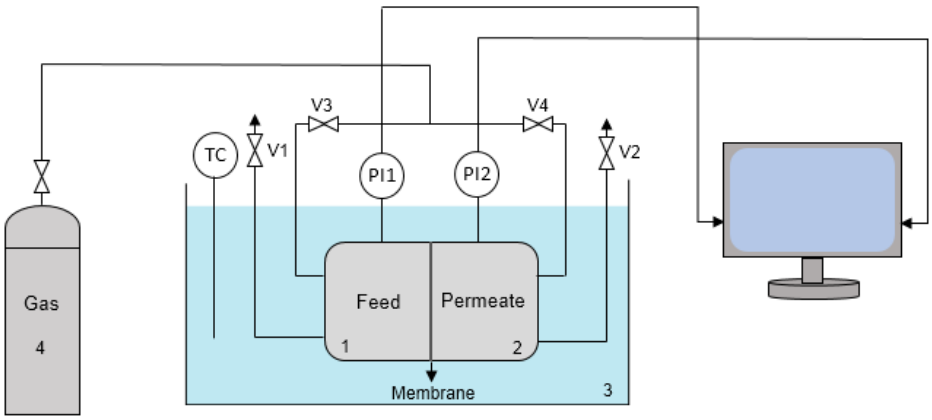

Figure 2.6 – Schematic of gas permeation apparatus (1 – Feed compartiment; 2 – Permeate compartment; 3 – Water bath; 4 – Feed Gas; TC – Temperature controller; PI1, PI2 – Pressure indicators; V1, V2 – Exhaust valves; V3, V4 –Inlet valves).

This apparatus consists in a permeation cell that is divided in two compartments with the same volume, corresponding to feed and permeate. The cell is emerged in a water bath at 30ºC, which is controlled by a thermostat (Julabo ED, Germany) and attached to the each of cell compartment is one transducer (Jumo type 404327, Germany), that measures the pressure in each compartment at every second. PicoLog software was used to monitor the pressure variation.

The membrane is placed between the two compartments and to guarantee that within the cell only the studied gas exists, with all valves open, a purge is made. After that, the exhaust valves are closed and a pressure of about 0.7 bar is settled. Reaching the desired pressure, the inlet valves are closed and the pressure is left stabilizing during a few minutes. When the pressure is stabilized, the permeate exhaust valve is rapidly opened and closed, generating a pressure difference between both cell compartments (driving force). After that, a gradually raise in the pressure on permeate compartment and a slowly decrease in the feed side is observed, until the equilibrium is reached.

For the permeability calculations, the time when the driving force is made is considered the time t_0. Gas permeability values were obtained through the analysis of both cell compartments pressure variation with time, using **Equation 2.7**. [66]

$$\frac{1}{\beta} \times \ln\left(\frac{\Delta P_0}{\Delta P}\right) = P \times \frac{t}{l} \qquad \textbf{(Eq. 2.7)}$$

Where,

β – Experimental cell geometric parameter (m^{-1})

ΔP_0 – Pressure difference at t_0 (bar)

ΔP - Pressure difference through time (bar)

P – Permeability ($m^2.s^{-1}$)

t – Time (s)

l – Membrane thickness (m)

Therefore, a graph representation of $\frac{1}{\beta} \times \ln\left(\frac{\Delta P_0}{\Delta P}\right)$ as a function of $\frac{t}{l}$ was made, in which the slope represents the membrane gas permeability.

The geometric parameter β, depends on the cell used and is given by **Equation 2.8**

$$\beta = A \times \left(\frac{1}{V_{Feed}} + \frac{1}{V_{Perm}}\right) \qquad \textbf{(Eq. 2.8)}$$

Where,

β – Geometric parameter (m^{-1})

A – Membrane area (m^2)

V_{Feed} – Feed compartment volume (m^3)

V_{Perm} – Permeate compartment volume (m^3)

In this work, cell geometric parameter was determined experimentally, using a PDMS membrane with a N_2 permeability already known of 2.075×10^{-10} $m^2.s^{-1}$ and with a thickness of 1.20×10^{-4} m. This calibration followed the same protocol as membrane permeation experiments. Thus, with the obtained pressure values through time, a graph representation of $\frac{1}{P} \times \ln\left(\frac{\Delta P_0}{\Delta P}\right)$ as a function of $\frac{t}{l}$, was made, where β value corresponded to the slope of this representation.

Ideal selectivity (α) is given by **Equation 2.9**

$$\alpha = \frac{P_A}{P_B} \qquad \textbf{(Eq. 2.9)}$$

Where,

α – Ideal selectivity

P_A – Permeability of A ($m^2.s^{-1}$)

P_B – Permeability of B ($m^2.s^{-1}$)

3. Results and discussion

This discussion is separated in two parts, the first one is relative to the pristine MOF and its derived MOF supporting ionic liquid (IL@MOFs) materials characterization and the second is relative to the mixed matrix membranes (MMMs) characterization.

3.1 Pristine MOF and IL@MOFs characterization

The IL@MOFs (ADILS7A, ADILS7B and ADILS8) are new materials synthesized at REQUIMTE-Porto. These materials were firstly validated also at REQUIMTE-Porto through powder X-ray diffraction and FTIR analyses (**Appendix 7.2**).

In this thesis in order to complement the characterization already performed to the materials, the IL@MOFs ADILS7A, ADILS7B and ADILS8 were firstly characterized by scanning electron microscopy (SEM) to evaluate their morphology. Along with MIL-101(Cr), they were also characterized by thermogravimetric analysis (TGA) and N_2 adsorption isotherm at 77K.

3.1.1 Scanning electron microscopy (SEM)

Scanning electron microscopy (SEM) allowed the visualisation and determination of the average particle size of the used materials. The images of ADILS7A, ADILS7B and ADILS8 powdered samples were obtained using a magnification of x6000, as shown in **Figure 3.1**.

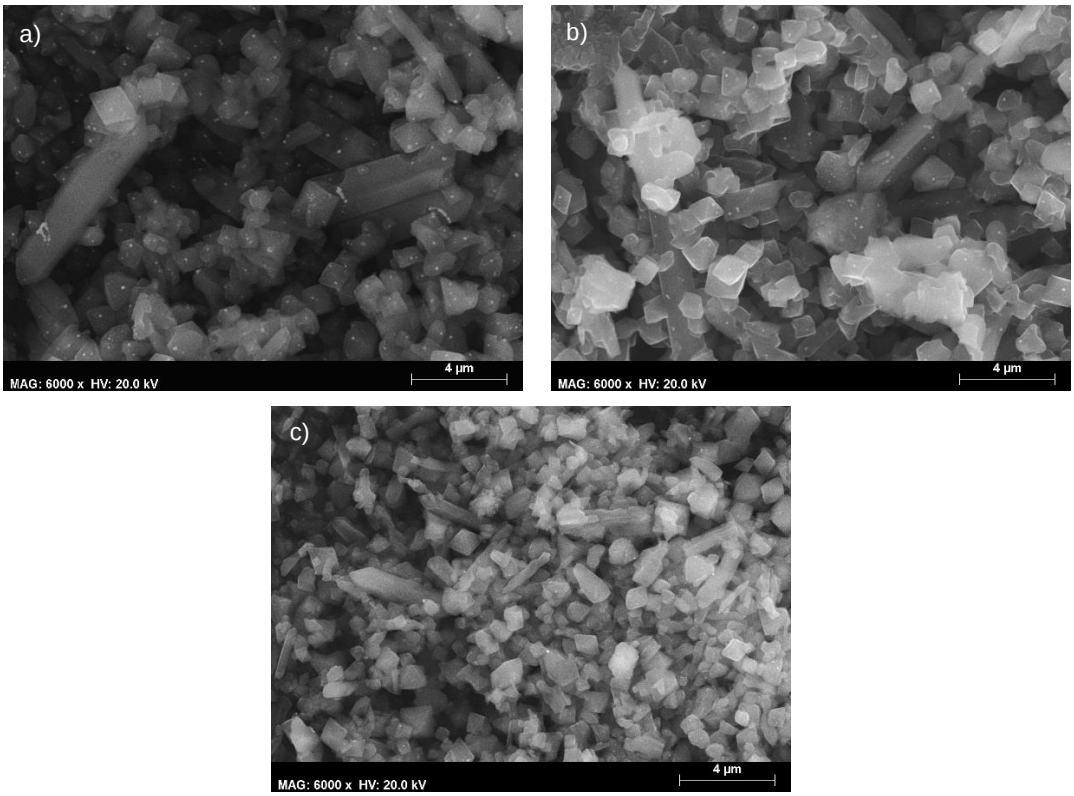

Figure 3.1 – SEM images (x6000) of the powders (a) ADILS7A, (b) ADILS7B and (c) ADILS8.

As can be seen in **Figure 3.1**, the particles of all materials do not present an homogeneous size, thus instead of determing the particle size as a mean, an interval of values was established. Therefore, the particle sizes of ADILS7A, ADILS7B and ADILS8 samples are within the intervals, 744nm – 8.96µm, 641nm – 6.36µm and 430nm – 4.63µm, respectively. Also, it is possible to see that most of the crystals of IL@MOF materials have an octahedron shape, which is characteristic of MIL-101(Cr) crystals (**Figure 3.2**).[67,68] This can indicate that MIL-101(Cr) mantained his morphology after the incorporation of the ionic liquids in its pourous structure.

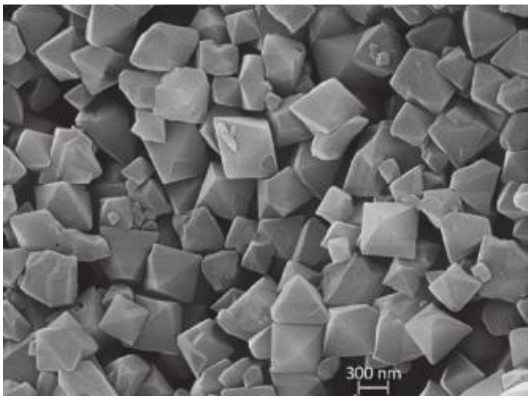

Figure 3.2 – SEM image of MIL-101(Cr) crystals from literature. [68]

3.1.2 Thermogravimetric Analysis (TGA)

TGA was performed to determine the thermal stability of the MOF MIL-101(Cr) and the IL@MOFs samples used in this work (ADILS7A, ADILS7B and ADILS8).

In **Figure 3.3** it is represented the TGA curves of MIL-101(Cr), ADILS7A, ADILS7B and ADILS8 powders.

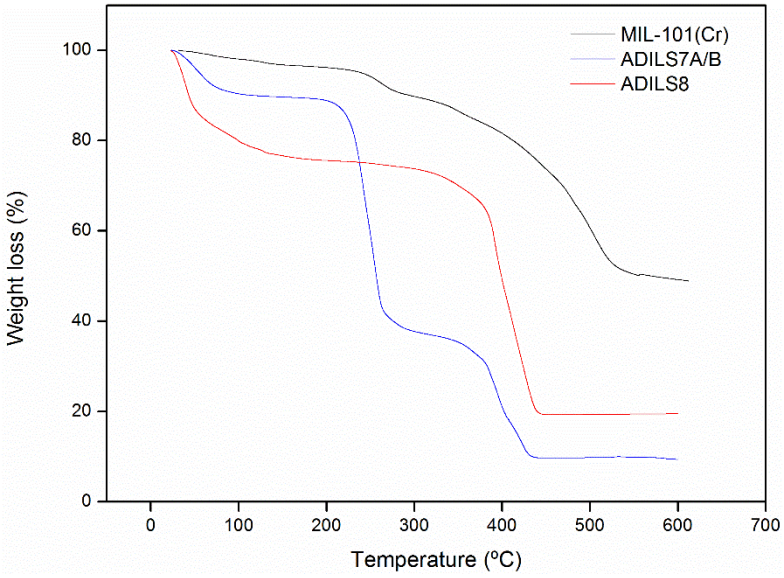

Figure 3.3 – Weight loss as a function of temperature of MIL-101(Cr), ADILS7A/B and ADILS8.

The TGA (**Figure 3.3**) shows that MIL-101(Cr) has two weight loss steps. The first one is in the range of 25-290ºC with about 10% weight loss, which may be due to the loss of guest water molecules and other impurities from its synthesis. The second step, corresponds to a weigh loss of about 40% in the range 320 to 545ºC, which is related with the elimination of OH/F groups that leads to the degradation of the framework.[69] Hence, this analysis indicates that MIL-101(Cr) is thermally stable up to 320ºC and if necessary should be activated at temperatures below this one. The obtained results are very similar to the ones reported in previous studies of MIL-101(Cr), in which the first weight loss step is near 10% and with a degradation temperature between 273 and 400ºC.[31,69,70]

ADILS7A and ADILS7B samples presented the same TGA profile and this phenomenon can be explained by the fact that these two materials have been incorporated by the same method in MIL-101(Cr) porous structure (**Appendix 7.1**). By the analysis of the TGA, these materials are more unstable than MIL-101(Cr), possessing three distinct weight loss steps. In the first one, a 10% weight loss occurs up to 90ºC, which can be related with the loss of guess water molecules or other impurities. Between 210 ºC and 275ºC a second weight loss of about 50% occurs, that may be due to the ionic liquid ([PMIM][Br]) degradation, which according to the literature is near 230ºC.[71] The last weight loss step occurs in the range of 320-435 ºC and may correspond to the MOF framework degradation.

The TGA of the ADILS8 sample shows that this material loses more weight, starting with a weight loss near to 20% until 100ºC, which may be due to the loss of guess water molecules or other impurities of its synthesis. A second weight loss of about 50% occurs between 300ºC and 445ºC, which may be explain by both ionic liquid and MOF degradation. In this case, it was not possible to distinguish between the IL and MOF since the ionic liquid degradation temperature is about 273ºC [72] which is near to the one of MIL-101(Cr).

3.1.3 Adsorption equilibria

In this work, the adsorption equilibrium isotherms were measured using three different approaches, namely the net adsorption (q_{net}), excess amount adsorbed (q_{ex}) and absolute adsorption (q_t) as described in **section 2.2.2**. For the calculation of q_t it is necessary to know some physical properties of the adsorbent. Hence, N_2 adsorption isotherm at 77K and helium picnometry analyses were performed, to determine the density and porous volume of the samples and, thus calculate the total adsorbed amounts of N_2 and CO_2 at 30ºC.

N_2 adsorption isotherm at 77K

The powders of MIL-101(Cr), ADILS7A, ADILS7B and ADILS8 were subjected to this analysis to determine their superficial area and pore volume. The results showed that both ADILS7A and ADILS7B samples did not possess any surface area. Thus, in **Figure 3.4** only shows the N_2 adsorption isotherms of MIL-101(Cr) and ADILS8 solids.

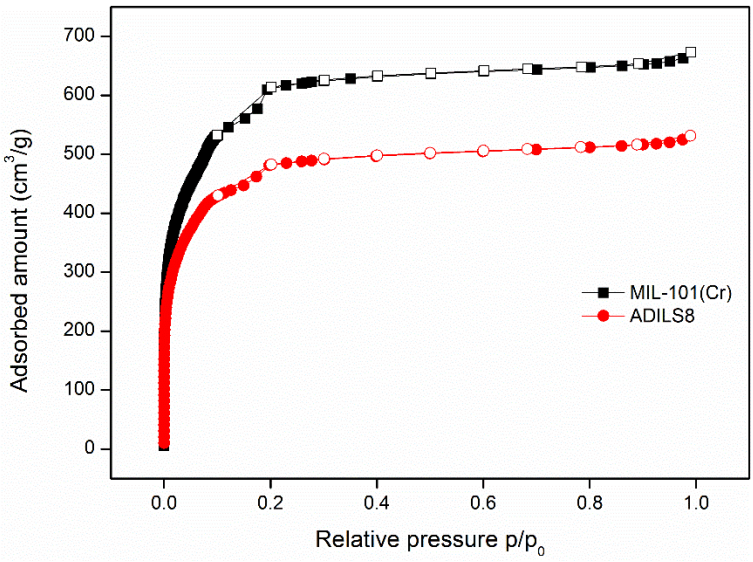

Figure 3.4 – N_2 adsorption/desorption isotherms at 77K of MIL-101(Cr) and ADILS8. Open/closed symbols denote desorption/adsorotion data.

MIL-101(Cr) and ADILS8 isotherms are similar, which according the IUPAC classification corresponds to an isotherm type-I. In addition, two secondary uptakes are observed, one near p/p_0=0.1 and one at p/p_0=0.2. This is typical of structures that possess two different sizes of microporous windows, which is the case of MIL-101(Cr).[31,73] Through the analysis of MIL-101(Cr) isotherm, a BET surface area of 2244 $m^2.g^{-1}$ and a pore volume of 1.03 $cm^3.g^{-1}$ at p/p_0~0.97 were determined. These values are similar to the ones reported in previous works.[31,67,74,75] With the addition of the ionic liquid, the values of both BET and pore volume decreased to 1853 $m^2.g^{-1}$ and 0.81 $cm^3.g^{-1}$ at p/p_0~0.98, respectively. This decrease was expected and is related with the presence of the ionic liquid within the porous structure of MIL-101(Cr).[70]

Helium picnometry

Since both ADILS7A and ADILS7B materials do not possess any surface area, they are not suitable for adsorption applications. Thus, only MIL-101(Cr) and ADILS8 samples were subjected to Helium picnometry. This technique, as described before in **section 2.2.2,** is used to determine the skeletal density of the materials. This parameter depends on the volume and mass of the sample and it is necessary to calculate the total adsorbed amount (q_t).

For its calculations, the same equations as for the adsorption/desorption equilibria isotherms are used (**section 2.2.2**), although in this case the helium act as an inert and it is not adsorbed by MIL-101(Cr) or ADILS8. Hence the material density (ρ_s) is given by the plot of sample weight as a function of gas density. Thus, the ρ_s is calculated through the material weight (W_A) and volume (V_A) average values, which are obtained from the intersection and slope of the fitting, respectively, after subtracting the weight and volume of the calibrated system cells.[34]

In **Figure 3.5** and **Figure 3.6** the sample weight as a function of the gas density for MIL-101(Cr) and ADILS8, respectively, is represented.

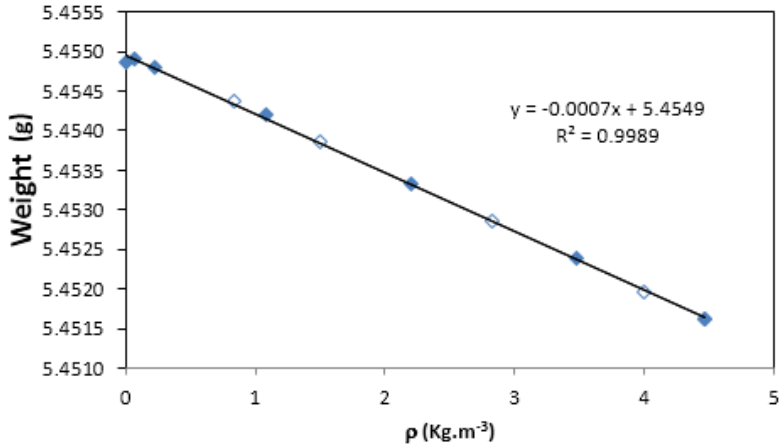

Figure 3.5 – Sample weight as a function of gas density for MIL-101(Cr).

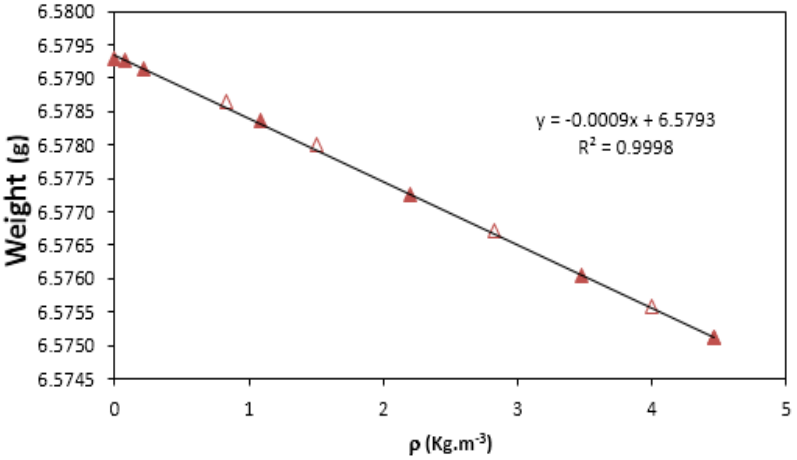

Figure 3.6 – Sample weight as a function of gas density for ADILS8.

The weight (W_A) and volume (V_A) average values of MIL-101(Cr) and ADILS8 are given in **Table 3.1**.

Table 3.1 – Weight (W_A) and Volume (V_A) average values of MIL-101(Cr) and ADILS8

	MIL-101(Cr)	**ADILS8**
W_A (g)	0.2507	0.1041
V_A (cm^3)	0.1439	0.0625

Thus, a skeletal density of 1.74 $g.cm^{-3}$ was obtained for MIL-101(Cr), which is in accordance with previous works.[76,77] Regarding the ADILS8 sample, a skeletal density of 1.66 $g.cm^{-3}$ was measured.

Adsorption/Desorption equilibria of CO_2 and N_2 at 30ºC

The adsorption equilibrium measurements of CO_2 and N_2 on MIL-101(Cr) and ADILS8 samples were carried out, since the main objective of this work was the capture of CO_2 from post-combustion streams. Both pure gases measurements were done at 30ºC within a pressure interval of 0 to 10 bar, in the gravimetric apparatus described in **section 2.2.2**. The desorption isotherm was measured to evaluate the material regeneration capability and the existence of hysteresis phenomena.

To facilitate the isotherms analysis, the adsorption and desorption points of all measured isotherms were taken in pressure ranges as similar as possible. All measured isotherms for N_2 and for CO_2 are type-I according to IUPAC classification [27], being the measurements checked for reproducibility. All data are reported in **Appendix 7.3**.

- **MIL-101(Cr)**

The MOF MIL-101(Cr) is a very good adsorbent for gas applications due to its good stability, high pore volume (mainly microporous) and easy regeneration. Also, it possesses unsaturated metal sites of Cr (III) that interact with CO_2 which has a high quadrupole moment (13.4×10^{-14} Cm^2), as well as a high polarizability (26.3×10^{-25} cm^3). Hence, it is expected higher uptakes of CO_2 when compared with N_2, which has a much lower quadruple moment and polarizability, 4.7×10^{-40} Cm^2 and 17.6×10^{-25} cm^3, respectively. [31,58,78]

Figure 3.7 presents the adsorption/desorption isotherms of N_2 and CO_2 at 30ºC in the three different approaches q_{net}, q_{ex} and q_t, already described in **section 2.2.2**. Moreover, for the absolute amount adsorbed calculations a pore volume (V_p) of 1.03 $cm^3.g^{-1}$ and a skeletal density (ρ_s) of 1.74 $g.cm^{-3}$, were used, as described earlier.

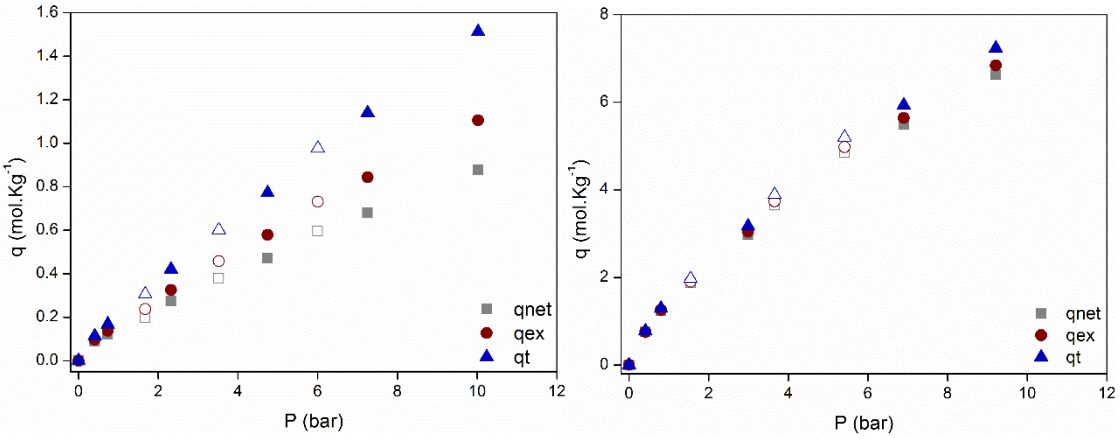

Figure 3.7 – N_2 (left) and CO_2 (right) adsorption isotherms on MIL-101(Cr) at 30ºC ■ qnet adsorption isotherm; ● qex adsorption isotherm; ▲ qt adsorption isotherm; closed/open symbols represent adsorption/desorption data).

Both CO_2 and N_2 adsorption/desorption equilibrium isotherms do not show any hysteresis effect, which means that for both gases the adsorbent has recovered totally to its initial clean state. Furthermore, it is possible to observe that at low pressures (< 1bar) the isotherms corresponding to the three different quantities (q_{net}, q_{ex} and q_t) are similar as expected; however as the pressure increases the isotherms start to diverge from each other, especially for N_2 adsorption isotherms. This phenomenon was explained in other works by the fact that at low pressures the gas bulk density of the adsorptive is much lower than the pore density.[29]

The differences between the q_{net}, q_{ex} and q_t approaches relies in the fact that in their calculation each approach takes into account different properties of the adsorbent. In the case of the adsorbed quantity q_{net} (**Equation 2.1**) it does not account with the structural properties of the adsorbent (skeletal density and pore volume), being the one that present the lowest values, which are independent of any further experimental measurements with a probe inert molecule such as Helium. The q_{ex} amount is calculated using the skeletal density of the adsorbent (**Equation 2.2**) and present higher values than q_{net}. The absolute or total quantity q_t is shown above the other quantities because besides the skeletal density of the adsorbent it also accounts with the pore volume of the sample (free space for gas diffusion) (**Equation 2.3**).

Figure 3.8 shows a comparison between our measurements and the ones from the literature at 25ºC[79], which is a temperature near to the one used in this work (30ºC).

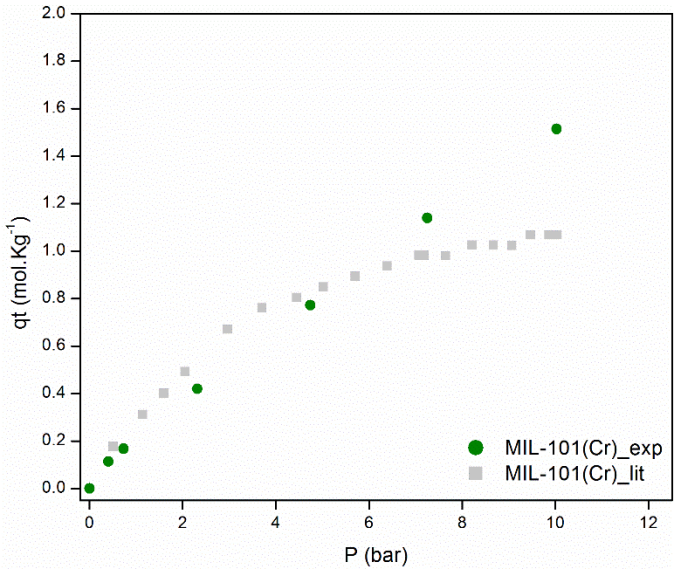

Figure 3.8 –N_2 adsorption isotherms on MIL-101(Cr) at 30ºC comparision with the literature at 25ºC. [79]

According to the only literature data for a pressure of approximately 10 bar at 25ºC a total amount adsorbed (qt) of 1.07 mol.Kg^{-1} was obtained. In this work, for the same pressure at 30ºC, a qt of 1.51 mol.Kg^{-1} was observed. This represent an increase of 1.4 times when comparing with literature data. However, our data were check for reproducibility and no other available works found similar experimental data to further complement this discussion.

Figure 3.9 shows a comparison of CO_2 adsorption equilibrium data with the literature [67], expressed in total amount adsorbed (q_t) on MIL-101(Cr) at 30ºC.

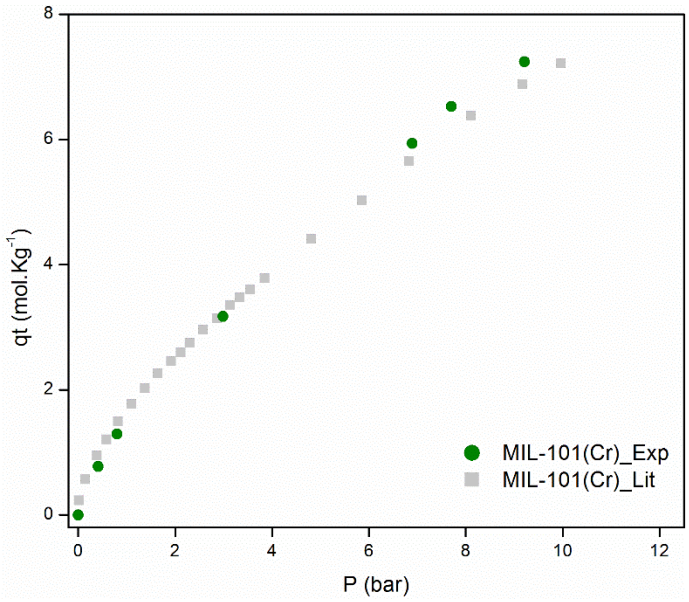

Figure 3.9 –Comparison between this work and literature CO_2 adsorption isotherms on MIL-101(Cr) at 30ºC. [67]

As seen in **Figure 3.9**, is possible to verify that our experimental CO_2 adsorption isotherm is similar to the one reported in the literature.[67] In fact, at 9.2 bar of pressure a q_t of 7.24 mol.Kg^{-1} was observed, which is similar to the amount reported (6.87 mol.Kg^{-1}) in the literature at the same pressure.[67]

Figure 3.10 shows the adsorption/desorption isotherms of N_2 and CO_2 on MIL-101(Cr) at 30ºC, expressed in total amount adsorbed (q_t).

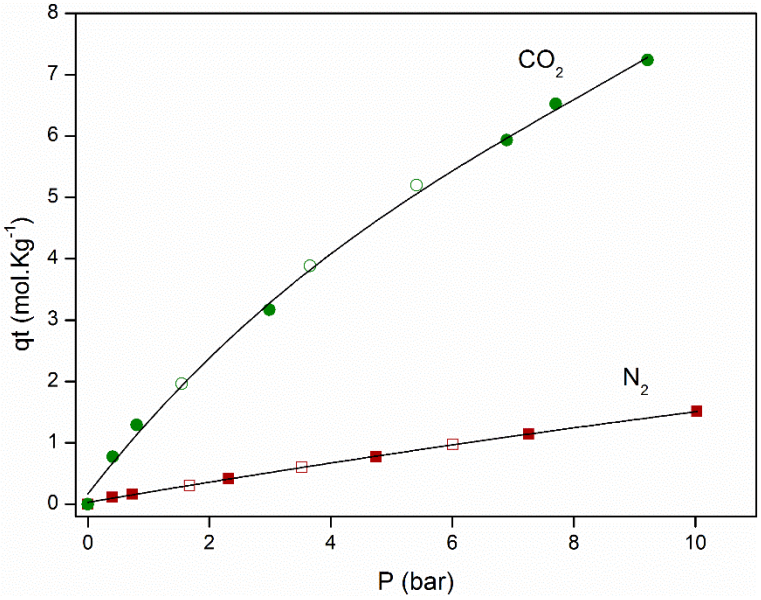

Figure 3.10 – N_2 and CO_2 adsorption/ desorption isotherms on MIL-101(Cr) at 30ºC (closed/open symbols denote adsorption/desorption data; the solid line are a quide to the eye).

As expected MIL-101(Cr) adsorb higher amounts of CO_2 than N_2 (**Figure 3.10**). At the maximum pressure used in this work (P~10 bar), for CO_2, a q_t of 7.24 mol.Kg^{-1} was obtained, while for N_2, a q_t of 1.51 mol.Kg^{-1} was observed, which is almost 5 times lower than the value of CO_2. This can be explained by the stronger interactions of the unsaturated metal sites of MIL-101(Cr) with the high quadrupole moment of CO_2.

In addition, the CO_2/N_2 equilibrium selectivity for in MIL-101(Cr) was calculated according to **Equation 2.4**, being represented in **Figure 3.11** as a function of pressure.

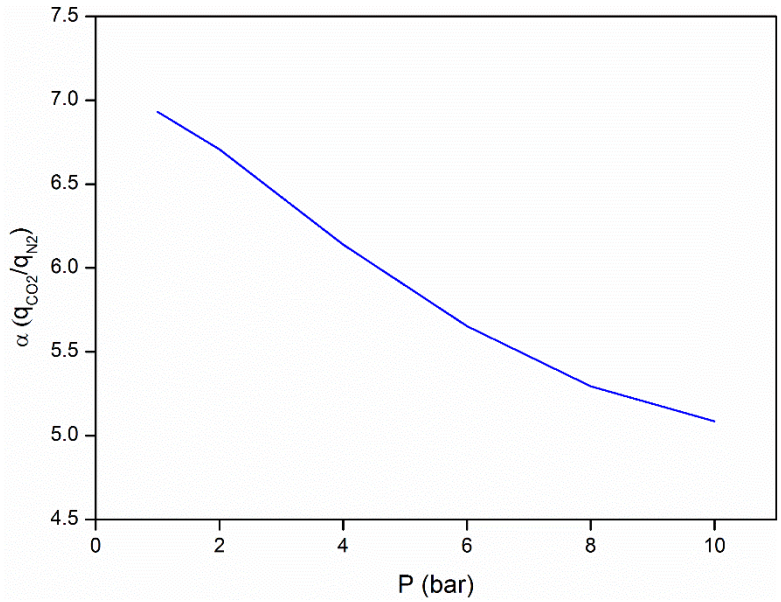

Figure 3.11 – CO_2/N_2 equilibrium selectivity in MIL-101(Cr) at 30ºC.

From **Figure 3.11**, it is possible to observe that with the increase of the pressure a decrease in the CO_2/N_2 ideal selectivity occurs. This result indicates that MIL-101(Cr) is a good candidate as an adsorbent material for CO_2 capture from post-combustion flue gas streams, which normally operates at low pressure values (near 1 bar).

- **ADILS8 ([BMIM][Br]@MIL-101(Cr))**

As previously mentioned, this material was obtained by the incorporation of the ionic liquid 1-butyl-3-methylimidazolium in the MIL-101(Cr) porous structure. Due to the tunable properties of ILs and MOFs as well as the large surface areas of these last ones, the system IL@MOF were exploited in this work as a potential adsorbent for gas adsorption, namely, for CO_2 adsorption. To the best of our knowledge, until this date does not exist any reports regarding adsorption/desorption equilibria of N_2 and CO_2 on [BMIM][Br]@MIL-101(Cr) systems.

Figure 3.12 shows the N_2 and CO_2 adsorption/desorption isotherms, represented in total amount adsorbed (q_t) as a function of pressure. The experimental data of the three different amounts (q_{net}, q_{ex} and q_t) for N_2 and CO_2 on ADILS8 sample are tabled in the **Appendix 7.3**.

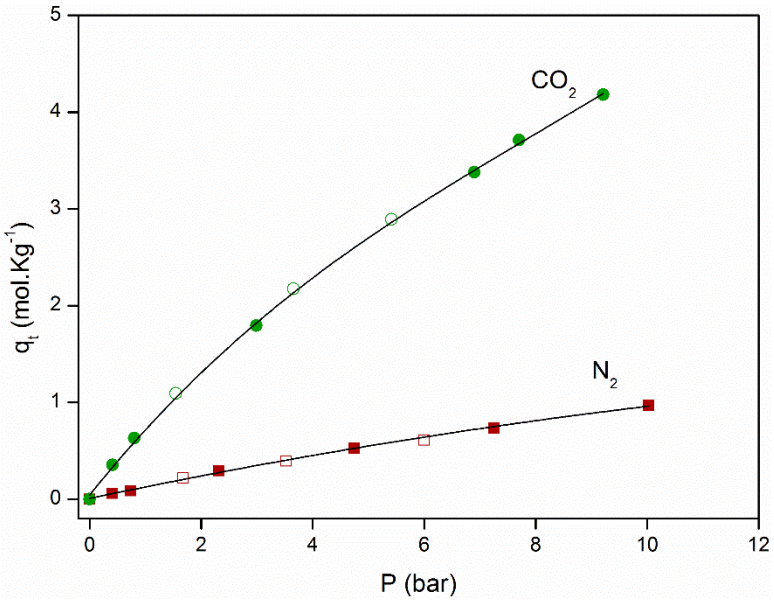

Figure 3.12 - N_2 and CO_2 adsorption/ desorption isotherms on MIL-101(Cr) at 30ºC (closed/open symbols denote adsorption/desorption data; the solid line are a quide to the eye).

According to the measure results, ADILS8 adsorbs higher amounts of CO_2 than N_2, following the same behaviour as MIL-101(Cr). For a maximum pressure near to 10 bar, a qt of 0.97 mol.Kg^{-1} and 4.18 mol.Kg^{-1}, were obtained for N_2 and CO_2, respectively. The adsorbed amount of N_2 is 4.3 times lower than the one of CO_2.

The CO_2/N_2 equilibrium selectivity for ADILS8 sample is shown in **Figure 3.13**.

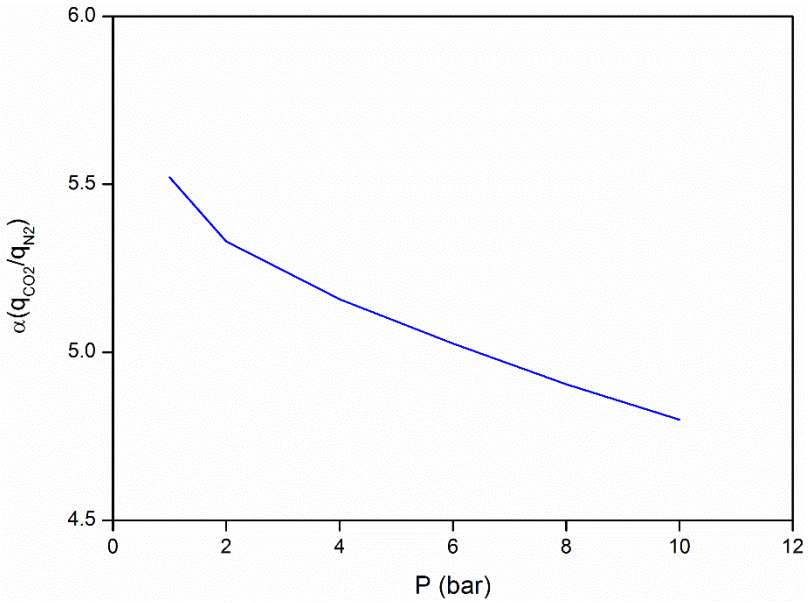

Figure 3.13 - CO_2/N_2 equilibrium selectivity in ADILS8 at 30ºC.

For the ADILS8 solid, the equilibrium selectivity as a function of pressure has a similar behaviour to the one found for MIL-101(Cr).

Figures 3.14 and **3.15** show a comparison between ADILS8 and MIL-101(Cr) adsorption/desorption isotherms of N_2 and CO_2, at 30ºC, and the CO_2/N_2 ideal selectivity, respectively.

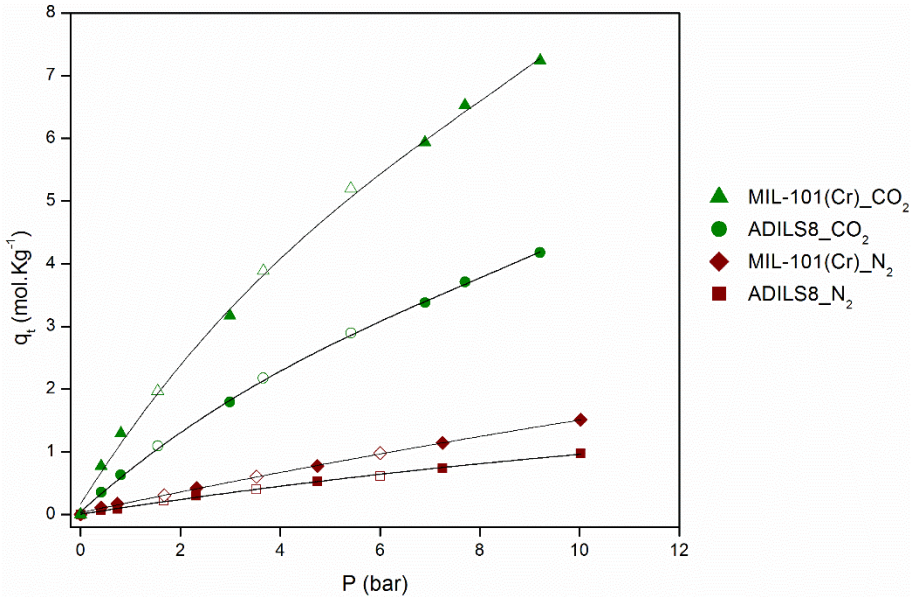

Figure 3.14 – N_2 and CO_2 adsorption/ desorption isotherms on MIL-101(Cr) and ADILS8 at 30ºC (closed/open symbols denote adsorption/desorption data; the solid line are a quide to the eye).

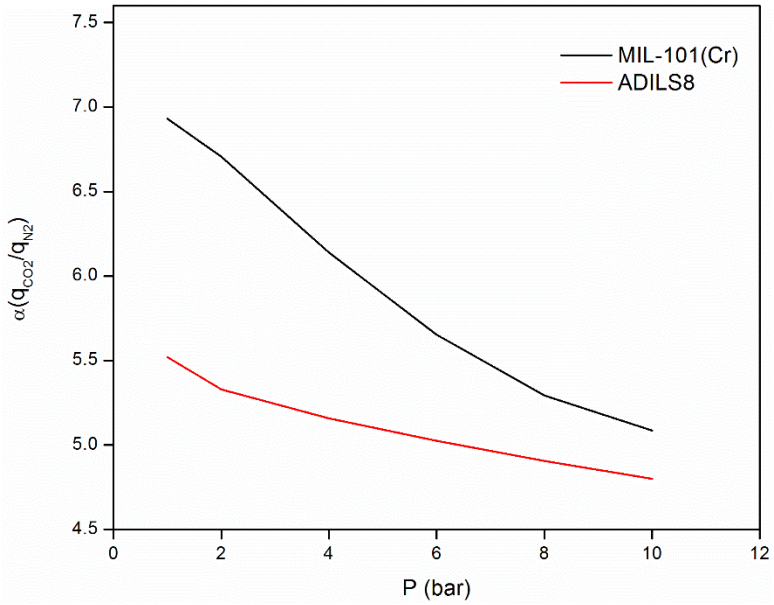

Figure 3.15 – CO_2/ N_2 ideal selectivity on MIL-101(Cr) and ADILS8 at 30ºC.

Both materials adsorb higher amounts of CO_2 than N_2, adsorbing both near 5 times more CO_2 than N_2. However, MIL-101(Cr) has higher CO_2 uptakes than ADILS8, adsorbing near 2 times more CO_2 (**Figure 3.14**). According to the literature data, the incorporation of an ionic liquid within

a MOF porous structure can lead to higher gas uptakes over the virgin MOF.[52,70] Therefore, in this work, ADILS8 lower uptakes of both N_2 and CO_2 compared to the results of MIL-101(Cr) suggests a high degree of pore filling with [BMIM][Br], that difficult the diffusion of gas molecules into the MIL-101(Cr) porous structure.[70] Nevertheless, some decrease in sorption capacity was expected, since part of the porous volume available for adsorption at the IL@MOF solid is occupied by the IL, in contrast with the pristine MIL-101(Cr). The question to answer was if that loss in capacity was small enough to still consider this IL@MOF approach interesting for capturing CO_2 by adsorption and further use it for membrane permeation. Furthermore, the CO_2/N_2 ideal selectivity of ADILS8 is near 1.3 times lower than MIL-101(Cr) at 1 bar, although with the increase of pressure this difference becomes quite smaller. Therefore, it can be concluded that the incorporation of the ionic liquid in the MOF porous structure did not enhanced the CO_2 adsorption capacity and CO_2/N_2 ideal selectivity, compared with the pristine MOF. Nevertheless, the optimization of the IL amount incorporation and its experimental methodology, namely decrease the IL/MOF quantity ration and improve the mixture homogeneity, are suggested as future work to advance further in this research.

3.2 Mixed matrix membranes characterization

The prepared membranes of Matrimid®5218, Matrimid®5218/MIL-101(Cr), Matrimid®5218/ADILS7B and Matrimid®5218/ADILS8 were characterized by Scanning Electron Microscopy (SEM), Energy-dispersive X-ray Spectroscopy (EDS), Contact angles, Mechanical properties, Thermogravimetric analysis (TGA) and Gas permeation with N_2 and CO_2.

3.2.1 Scanning Electron Microscopy (SEM)

Scanning electron microscopy (SEM) analysis allows the observation of the membrane morphology, being possible to evaluate the success of the interaction between the polymer and the filler. In this analysis, images of the surface and cross section of the prepared membranes, were obtained, using different magnifications (x1.000 and x3.000). The follow images present the surface and the cross section of the prepared membranes with a magnification of x1.000 and x3.000, respectively.

Figure 3.16 shows the surface and cross section SEM images of the Matrimid®5218 with different degrees of incorporation of MIL-101(Cr) (10%(w/w), 20%(w/w) and 30%(w/w)).

%(w/w) MIL-101(Cr)	Surface	Cross Section
0%	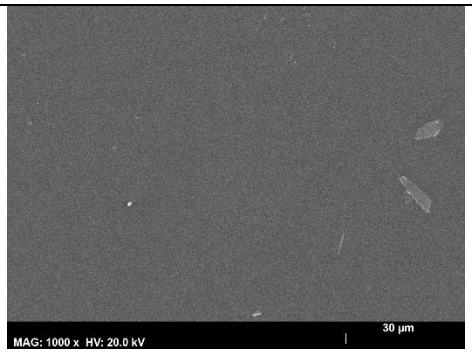	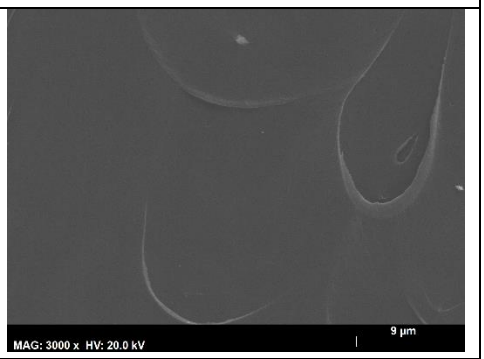
10%	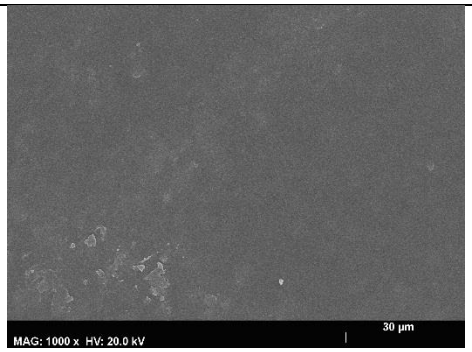	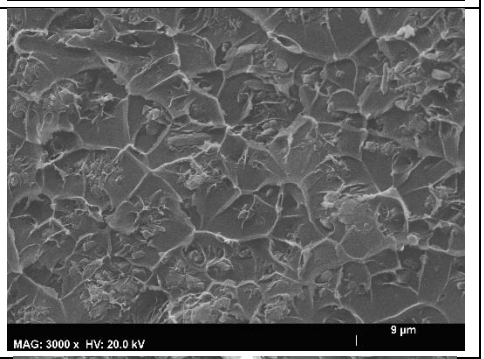
20%	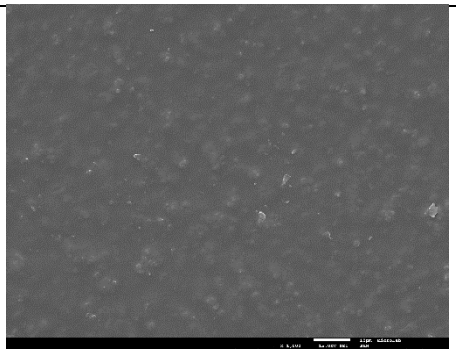	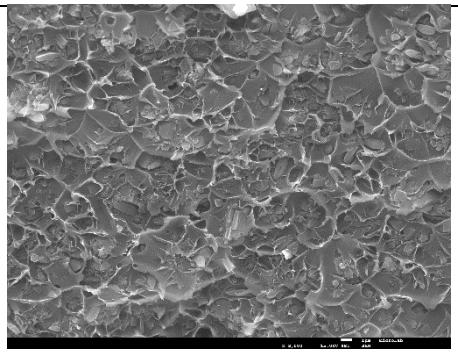
30%	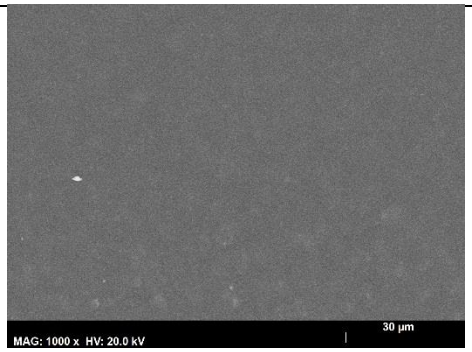	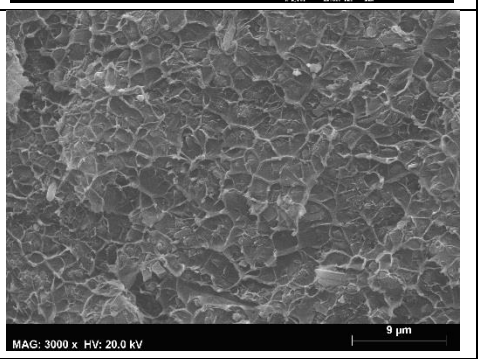

Figure 3.16 –SEM images of 0%, 10%, 20% and 30%(w/w) Matrimid® 5218/ MIL-101(Cr) membranes surface and cross section, with a magnification of x1000 and x3000, respectively.

The membrane composed by Matrimid®5218 (represented as 0%(w/w) MIL-101(Cr)), presents a homogeneous surface without the formation of agglomerates, as for the cross section images, it is possible to observe a dense structure without deformations, which is common for this type of membranes.[80]

Regarding Matrimid®5218/MIL-101(Cr) membranes, they all also possess homogenous surfaces without the presence of any deformations or agglomerates. These results can indicate a good dispersion of the MOF in the polymeric matrix. From the analysis of cross-section images is possible to observe that besides a dense structure, the membranes exhibit crater-like patterns with the MOF particles in the middle. This type of morphology was reported in other works as a result of plastic deformation, which is caused by the surface tensions that are created due to the high affinity between the filler and the polymer matrix. [44,57]

Matrimid®5218/ADILS7B membranes surface and cross section SEM images are represented in **Figure 3.17**.

% (w/w) ADILS7B	Surface	Cross Section
10%	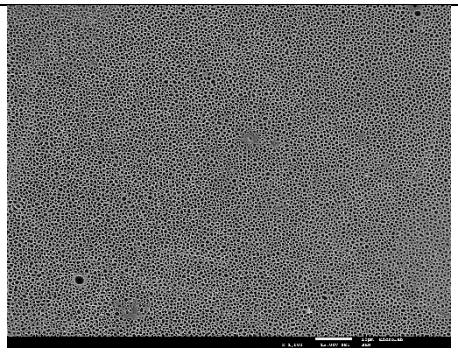	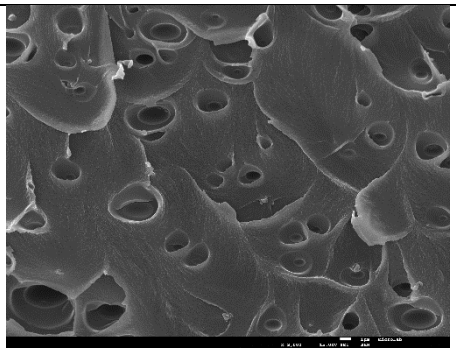
20%	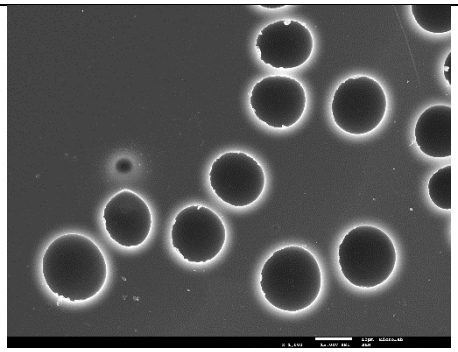	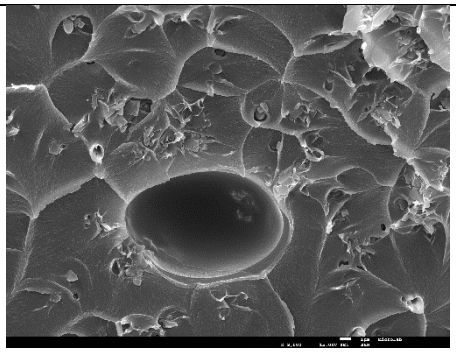
30%	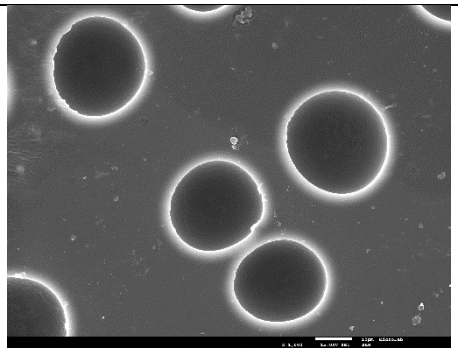	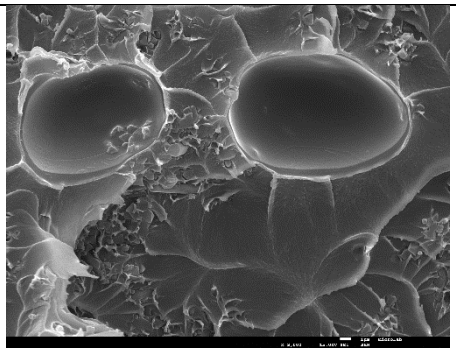

Figure 3.17 – SEM images of 10%, 20% and 30%(w/w) Matrimid®5218/ADILS7B membranes surface and cross section with a magnification of x1000 and x3000, respectively.

From **figure 3.17** it is possible to observe that the surface of Matrimid®5218+10%ADILS7B membrane is full of cavities and these cavities are also observed in the cross-section images. For the other loadings of ADILS7B in the polymeric matrix some cavities in the surface are also observed, which increases with an increase of IL@MOF loading. For their cross-section images, it is observed a dense structure with cavities, although in less quantity than in Matrimid®5218+10%ADILS7B membrane. A crater like type morphology with the IL@MOF crystals in the middle it is also visible, which indicates the existence of plastic deformation, meaning that ADILS7B also has a good interaction with Matrimid®5218. [44,57]

% (w/w) ADILS8	Surface	Cross Section
10%	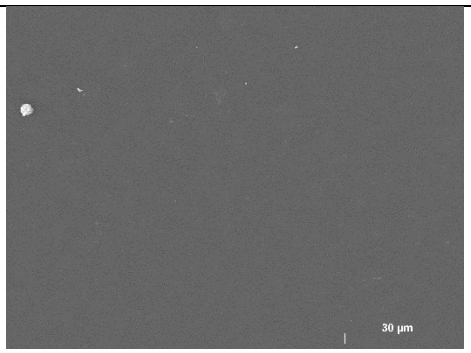	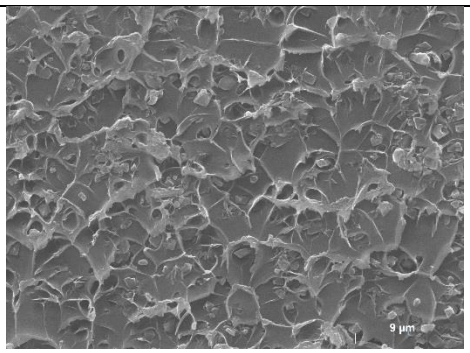
20%	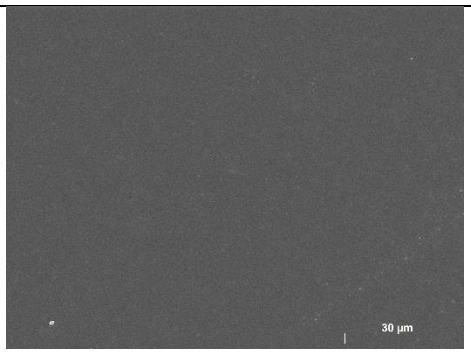	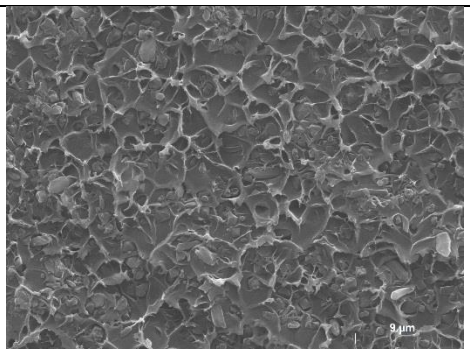
30%	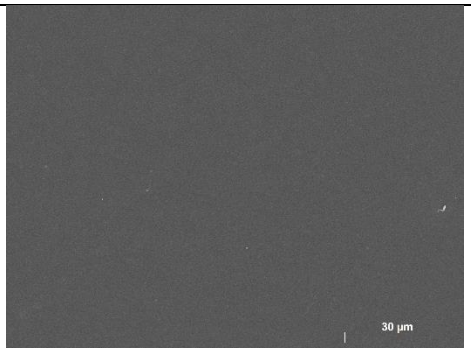	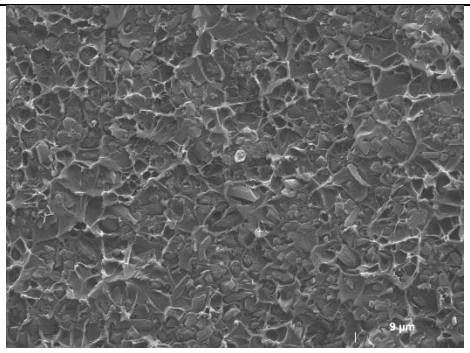

Figure 3.18 - SEM images of 10%, 20% and 30%(w/w) Matrimid®5218/ADILS8 membranes surface and cross section with a magnification of x1000 and x3000, respectively.

In **Figure 3.18** it is possible to observe that the ionic liquid incorporation within the MIL-101(Cr) by the ship-in-bottle method did not change the membranes morphology. Hence, for all the prepared Matrimid®5218/ADILS8 membranes a homogenous surface without any deformations is observed. Moreover, the cross-section images of all membranes present a dense

structure, without the presence of non-selective voids where it can be seen a crater-like patterns with the ADILS8 particles in the middle. This phenomenon, can indicate that ADILS8 has a good affinity to Matrimid®5218 polymer.

Nevertheless, all the prepared membranes have a dense structure, which is one of the requisites for gas separation in CO_2 capture processes, as well as a good interaction between the polymer and filler. This interaction is crucial for the MMMs success, because one of the main factors that affects the transport properties of the membranes is the formation of non-selective voids and a good interaction between polymer and filler.[81] Therefore, the prepared membranes can be used in the gas permeation experiments.

3.2.2 Energy-Dispersive X-Ray Spectroscopy (EDS)

The energy-dispersive x-ray spectroscopy (EDS) analysis (described in **section 2.2.6**) was made to guarantee the presence of the incorporated material on the membrane as well as its dispersion on the membrane surface, through elemental identification. This analysis was done to all MIL-101(Cr) and ADILS8 percentages of incorporation in the polymer matrix (10% (w/w), 20%(w/w), 30%(w/w)). MIL-101(Cr) was identified by the detection of Chromium and the ionic liquid [BMIM][Br] by the detection of Bromide.

Figure 3.19 shows the EDS element identification and X-ray mapping on chromium of Matrimid®5218/MIL-101(Cr) membranes.

%(w/w) MIL-101(Cr)	Elemental identification	X-ray mapping
10%	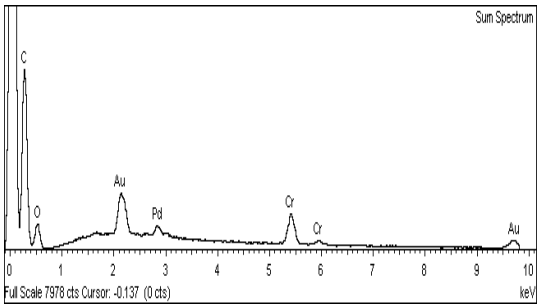	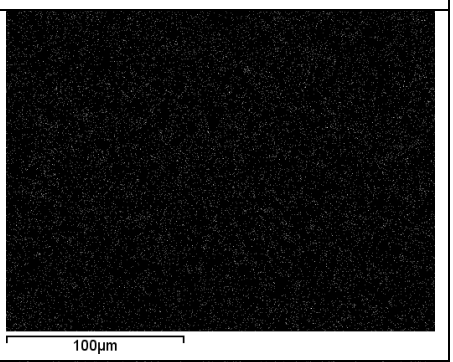
20%	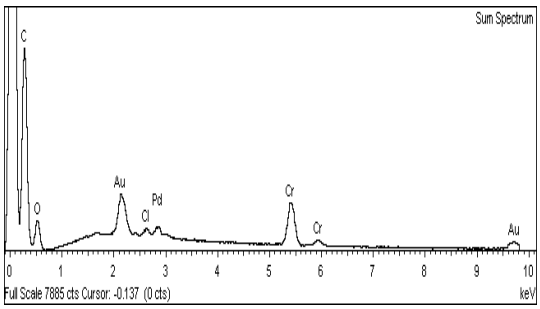	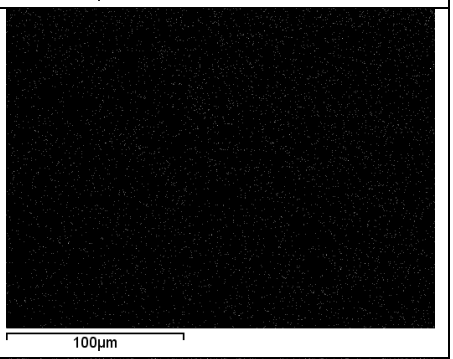
30%	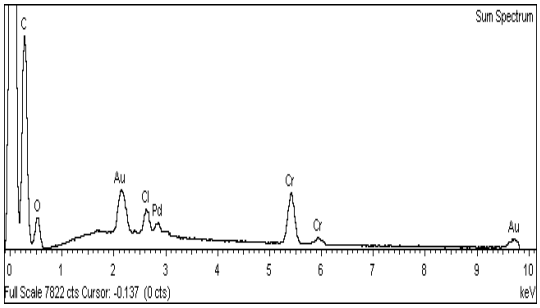	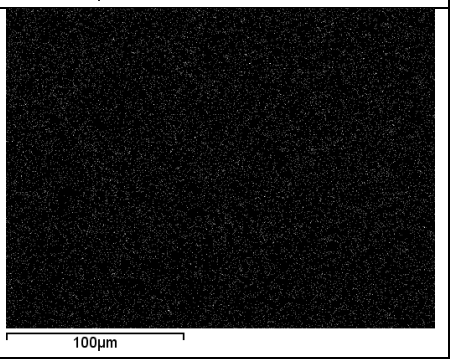

Figure 3.19 - EDS element identification and X-ray mapping of chromium on 10%, 20% and 30%(w/w) Matrimid®5218/MIL-101(Cr) membranes.

In the elemental identification images, two peaks of chromium are observed for all loadings of MOF, which ensures the presence of MIL-101(Cr) in the prepared membranes. In addition to chromium, gold (Au) and palladium (Pd) peaks also appear in the spectrum with a certain degree of intensity. Their appearance is due to the necessity of covering the samples with a layer of Au-Pd in order to realise the analysis. Regarding the X-ray mapping images, the white dots represent the chromium element. Hence it can be observed a good dispersion of MIL-101(Cr) on the membrane surface without the formation of agglomerates.

Figure 3.20 shows the EDS element identification and X-ray mapping on bromide of Matrimid®5218/ADILS8 membranes. In this case, for bromide identification it is necessary to change to scale from 10 keV to 20keV, because for lower values the bromide element is

overlapped with Au element, which is used in the cover layer applied on the samples. Therefore, it is only possible to detect the bromide element at 11keV.

%(w/w) ADILS8	Elemental identification	X-ray mapping
10%	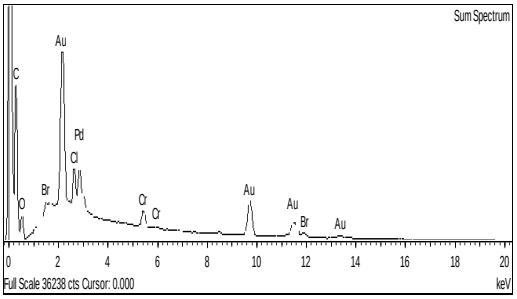	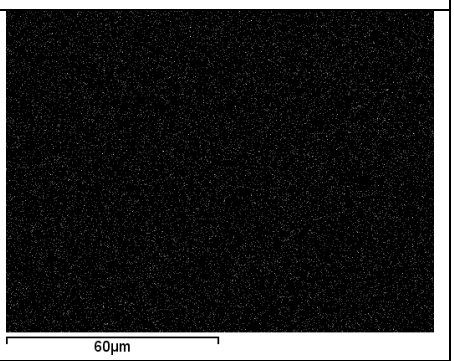
20%	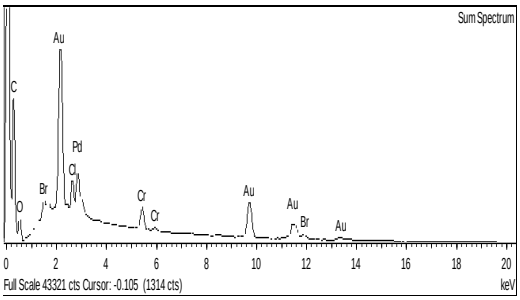	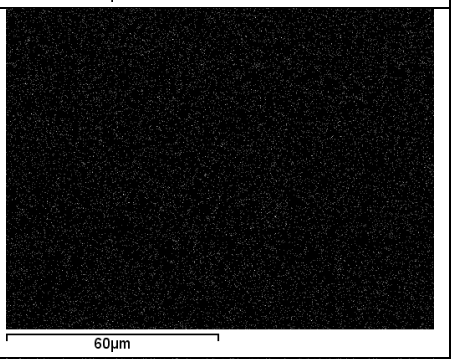
30%	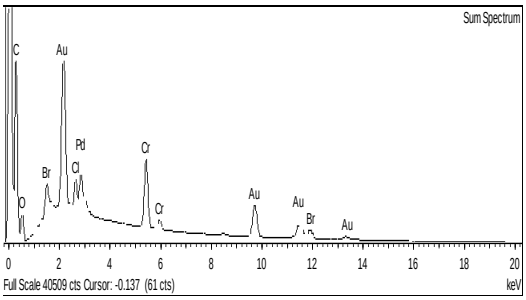	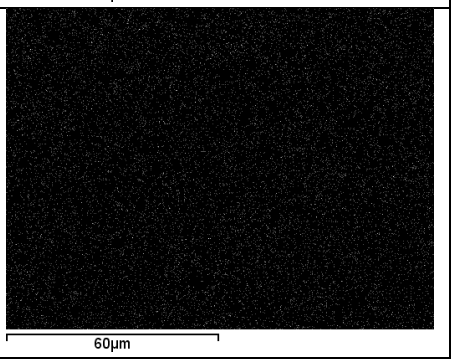

Figure 3.20 – EDS element identification and X-ray mapping of bromide on 10%, 20% and 30%(w/w) Matrimid®5218/ADILS8 membranes.

In **Figure 3.20** can be observed the appearance of both bromide and chromium elements to all incorporation percentages of ADILS8, verifying the presence of [BMIM][Br] and MIL-101(Cr) in the membranes. Through the X-ray mapping images, it is possible to observe a good dispersion of the bromide element (white dots), indicating a good dispersion of the ionic liquid in the membrane surface. Unfortunately, it was not possible to represent the dispersion of both [BMIM][Br] and MIL-101(Cr) on the same X-ray mapping image. Thus, the MIL-101(Cr) X-ray mapping images are represented in **Appendix 7.4**, in which a homogenous dispersion of the MOF is observed. Once more, a good dispersion of the filler without the formation of agglomerates is observed.

In addition, it is possible to observe that in the elemental analysis, besides the presence of Au and Pd, which are the elements that composed the samples coverage layer, chlorine (Cl) bands also appear on the spectrum. Since the solvent used in the preparation of the mixed matrix membranes was dichloromethane, the appearance of Cl can indicate that some solvent (dichloromethane) remained in the membranes.

In both Matrimid®5218/MIL-101(Cr) and Matrimid®5218/ADILS8 membrane group, the filler is homogeneously dispersed in the polymer matrix, which means that exists a good interaction between both phases. These results are in accordance with the ones obtained by SEM analysis (**section 3.2.1**), which also have shown the existence of a very good interaction between the polymer and filler.

3.2.3 Contact Angles

The contact angles measurements (described in **section 2.2.7**) were done in order to evaluate the membranes hydrophilicity. In this work, the measurements were made using water, being the membranes classified as hydrophilic if the measured contact angle is inferior to 90º and hydrophobic if the angle is superior to 90º.

Figure 3.21 shows the contact angles results of Matrimid®5218, Matrimid®5218/MIL-101(Cr), Matrimid®5218/ADILS7B and Matrimid®5218/ADILS8 membranes.

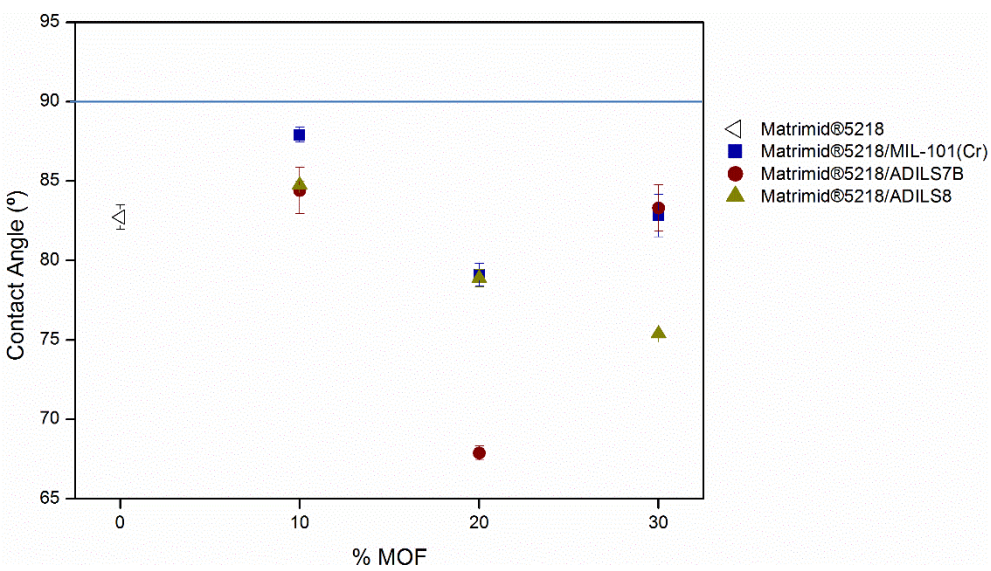

Figure 3.21 – Contact angles of Matrimid®5218, Matrimid®5218/MIL-101(Cr), Matrimid®5218/ADILS7B and Matrimid®5218/ADILS8 membranes.

Matrimid®5218 membrane showed to be hydrophilic with a contact angle of 83º, which is in accordance with previous reported values.[82,83] With the incorporation of MIL-101(Cr), the membranes turn more hydrophilic except for a 10% loading of MIL-101(Cr). In addition, the Matrimid®5218+20%MIL-101(Cr) membrane was the one that presented a more hydrophilic character, with a contact angle of 79º. Although the inexistence of a tendency in the obtained

values, an increase of hydrophilicity of the Matrimid®5218/MIL-101(Cr) membranes compared with the Matrimid®5218 membrane was expected due to the MIL-101(Cr) particles hydrophilic character.[38,84]

Regarding Matrimid®5218/IL@MOF membranes it is possible to observe that are all hydrophilic. In the case of ADILS7B membranes, the most hydrophilic membrane corresponds to a 20% loading of the IL@MOF in the membrane, with a contact angle of 68º. This value can be related with the increase in size of the cavities observed in the SEM images (**section 3.2.1**). For ADILS8 membranes a constantly increase in hydrophilicity with the increase of the IL@MOF concentration in the polymeric matrix, is observed. Furthermore, all IL@MOF membranes are more hydrophilic than both Matrimid®5218 and Matrimid/MIL-101(Cr) membranes, when comparing the same percentages of incorporation in the polymeric matrix. These results, can be associated with the high hygroscopic nature of both [PMIM][Br] and [BMIM][Br] [71] and the hydrophilic character of MIL-101(Cr), which together can enhance the hydrophilic properties of the membranes.

3.2.4 Mechanical properties

In this work, through the puncture test (described in **section 2.2.8**) the tensile strength of the prepared membranes was determined. Normally, through this technique the elongation of the material is also determined, however all the prepared membranes upon force application did not elongate, turning impossible the elongation calculations.

Matrimid®5218 is known to be a polymer with very good mechanical properties [55,56]. Hence, the objective of this work was to observe the modifications on the mechanical properties with the incorporation of MOF and IL@MOF in the polymer matrix.

As an illustrative example, the obtained data of the force (N) for Matrimid+10%MIL-101(Cr), Matrimid+20%ADILS7B and Matrimid+30%ADILS8 membranes, as a function of the distance (mm) is represented in **Appendix 7.5**. Through **Equation 2.5** and **Equation 2.6** the tensile strength necessary to puncture the membranes was calculated. Also, since the prepared membranes possess different thicknesses in order to make a viable comparison between them, the normalized tensile strength was determined. The obtained results of Matrimid®5218/MIL-101(Cr), Matrimid®5218/ADILS7B and Matrimid®521/ADILS8 membranes are in **Table 3.2**, **Table 3.3** and **Table 3.4** respectively.

Table 3.2 – Puncture test results (thickness, tensile strenght and normalised tensile strenght) of Matrimid®5218/MIL-101(Cr) membranes

%MIL-101(Cr)	Thickness (µm)	Tensile strength (MPa)	Normalised tensile strength (MPa/mm)
0%	163± 0.002	16.83 ± 0.52	103.03
10%	35 ± 2.95	3.00 ± 0.07	85.36
20%	56 ± 3.91	1.35 ± 0.10	23.95
30%	82 ± 5.07	0.80 ± 0.06	9.79

Table 3.3 – Puncture test results (thickness, tensile strenght and normalised tensile strenght) of Matrimid®5218/ADILS7B membranes

%ADILS7B	Thickness (µm)	Tensile strength (MPa)	Normalised tensile strength (MPa/mm)
10%	42 ± 4.21	4.79 ± 0.04	115.07
20%	34 ± 2.74	3.72 ± 0.21	106.08
30%	57 ± 2.54	2.85 ± 0.21	50.08

Table 3.4 – Puncture test results (thickness, tensile strenght and normalised tensile strenght) of Matrimid®5218/ADILS8 membranes

%ADILS8	Thickness (µm)	Tensile strength (MPa)	Normalised tensile strength (MPa/mm)
10%	50 ± 3.26	4.07 ± 0.20	80.82
20%	65 ± 1.37	2.12 ± 0.07	32.63
30%	61 ± 4.07	1.22 ± 0.01	20.25

The Matrimid®5218 membrane presented a tensile strength of 16.8 MPa, which is very similar to other values already reported for the same polymer, in which a tensile strength of 14.9 MPa was observed for a membrane with a thickness of 155 µm.[85] Thus, as expected the produced Matrimid®5218 membrane has a good flexibility and resistance.

With the addition of MIL-101(Cr) in the polymeric matrix, the tensile strength of the prepared membranes decreased when compared to Matrimid®5218 membrane (**Table 3.2**). In addition, it is possible to observe that the tensile strength of the membranes decreases with the increase of MIL-101(Cr) percentage in the polymeric matrix, which can indicate that the presence of MOF crystals turns the membranes more rigid. Usually this behaviour can be associated to the formation of MOF agglomerates in the polymer matrix.[85] However, EDS analysis (**section 3.2.2**), showed a good dispersion of MIL-101(Cr) in the membranes surface without the existence of MOF agglomerates and the cross section images of the SEM analysis (**section 3.2.1**) also showed a good dispersion of the MOF crystals . Thus, these results can be a consequence of the occurrence of plastic deformation caused by MIL-101(Cr) crystals.[86] Previous studies using MIL-101(Cr) as well as Fe(BTC) and Cu-BPY-HFS also showed a decrease in the tensile strength with the addition of the MOF in the polymeric matrix when compared to the polymeric membrane.[80,86,87] Therefore, it can be concluded that the incorporation of MIL-101(Cr) in the polymeric matrix

is not advantageous for the mechanical properties of the membranes, turning them more rigid and fragile.

Regarding Matrimid®5218/ADILS7B membranes (**Table 3.3**), a normalized tensile strength of 115.07 MPa/mm is observed for a 10% loading of the IL@MOF in the polymeric matrix. This value is higher than the ones of both Matrimid®5218+10%MIL-101(Cr) and Matrimid®5218 membrane, showing that the incorporation of [PMIM][Br] in the MOF porous structure turn the membranes more flexible. However, with the increase of ADILS7B loading in the membranes, a decreased is observed, being the highest tensile strength achieved for a 10% loading in the polymeric matrix. This behaviour, can be associated to the presence of a higher concentration of MIL-101(Cr) crystals, which already shown to turn the membrane more fragile. However, when compared to the values of Matrimid®5218/MIL-101(Cr) membranes, the values are still higher, which is an indication that the presence of the ionic liquid can act as a plasticizer in the polymeric matrix.

In the case of Matrimid®5218/ADILS8 membranes, similar results to MIL-101(Cr) are observed, occurring a decrease in the tensile strength with the incorporation of ADILS8 in the polymeric matrix. For higher loadings of IL@MOF the normalized tensile strength values are higher than the ones obtained for the same incorporation degree of MIL-101(Cr), which shows that the presence of [BMIM][Br] turn the membranes more flexible.

Previous studies with IL@MOF/Polymer membranes, namely using ZIF-8 as filler and the ionic liquid [BMIM][Tf_2N], also showed an improvement on the mechanical properties compared with the MOF/Polymer membranes.[88] However, for these particular IL@MOF systems any data concerning their effect on the MMMs mechanical properties were available. Therefore, it is possible to conclude that both [PMIM][Br] and [BMIM][Br] incorporation in MIL-101(Cr) porous structure improve the mechanical properties of the mixed matrix membranes, turning them more resistant and flexible. Also, [PMIM][Br] seems to be more advantageous to the enhancement of MIL-101(Cr) membranes mechanical properties than [BMIM][Br]. However, the ionic liquid quantity present in ADILS8 ([BMIM][Br]@MIL-101(Cr)) was not determined, turning impossible a feasible comparison between both ionic liquids.

3.2.5 Thermogravimetric Analysis (TGA)

Thermogravimetric analysis was used in order to evaluate the stability of the prepared membranes at high temperatures since the objective is to prepare mixed matrix membranes to use in post-combustion flues streams, which are normally between 100-200ºC.[89] Thus, to guarantee that they are suitable for being use in these streams, the membranes were submitted to a temperature raise until 300ºC.

In **Figure 3.22** and **Figure 3.23** the results of Matrimid®5218/MIL-101(Cr) and Matrimid®5218/ADILS8 membranes, respectively, are represented.

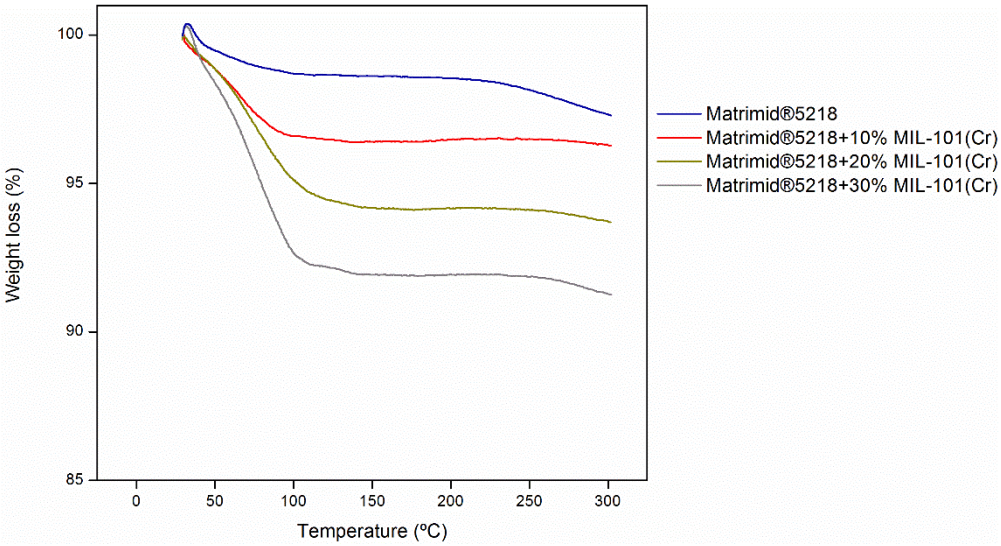

Figure 3.22 – Weight loss as a function of temperature of Matrimid®5218 and Matrimid®5218/MIL-101(Cr) membranes.

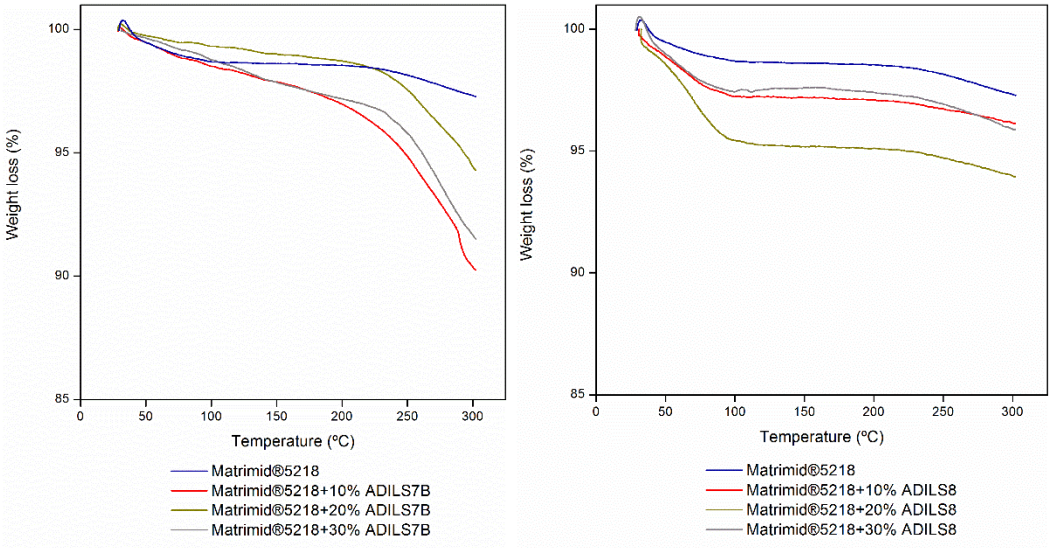

Figure 3.23 – Weight loss as a function of temperature of Matrimid®5218, Matrimid®5218/ADILS7B and Matrimid®5218/ADILS8 membranes.

Through the analysis of **Figure 3.22** it is possible to observe that Matrimid®5218 membrane has a total weight loss lower than 3% until 300ºC. This decrease can be related with the evaporation of water guest molecules and probably residual solvent (dichloromethane), which boiling point is at 40ºC[85]. This behaviour shows that the Matrimid®5218 membrane possess high stability up to 300ºC, which was expected since Matrimid polymer degradation temperature (T_d) starts near 440 ºC.[90]

Regarding Matrimid®5218/MIL-101(Cr) membranes a more unstable behaviour is observed than Matrimid®5218 membrane. Also, it is verified that with the increase in MIL-101(Cr)

loading in the membrane there is an increase in the weight loss up to 100ºC. Hence for the Matrimid®5218+30%MIL-101(Cr) membrane a weight loss near 8% is observed which is due to the loss of guest water molecules and residual solvent. Until 300ºC no other significant weight losses are observed, which was already expected since, as can be seen in the TGA of MIL-101(Cr) powder (**section 3.1.2**), this material does not reach its degradation temperature before 300ºC, being the decrease observed only due to the evaporation of water and other impurities.

For Matrimid®5218/ADILS7B membranes (**Figure 3.23**) a similar behaviour to Matrimid®5218 membrane is verified up to 100ºC, being more stable than MIL-101(Cr) membranes. After this temperature, all Matrimid®5218/ADILS7B membranes kept losing weight, gradually. However, this decrease only turns significant after reaching the 220ºC. This weight loss (~10%) is, according to ADILS7B powder TGA (**section 3.1.2**), explained by the beginning of the ionic liquid degradation. However, since the weight loss is very low, the membranes can be considered stable up to 300ºC. In the case of Matrmid®5218/ADILS8 membranes they also showed to be more stable than MIL-101(Cr) membranes, being the Matrimid®5218+20%ADILS8 membrane the most unstable with a total weight loss near to 5% up to 300ºC. These results are in accordance with the ADILS8 TGA (**section 3.1.2**), in which up to 300ºC only losses of water and impurities are observed.

In conclusion, all membranes showed to be stable up to 300ºC. which means that they all can withstand post combustion temperature conditions. Furthermore, the incorporation of the ionic liquid in the MOF turned the membranes more stable when compared to the ones with only MIL-101(Cr).

3.2.6 Gas Permeation

In this work, since the objective is the development of mixed matrix membranes for CO_2 capture from post-combustion processes, gas permeability experiments for the pure gases N_2 and CO_2 were carried out.

Figure 3.24 shows the obtained results of the gas permeation experiments of Matrimid®5218, Matrimid®5218/MIL-101(Cr), Matrimid®5218/ADILS7B and Matrimid®5218/ADILS8 membrane groups, for the pure N_2 and CO_2 pure gases.

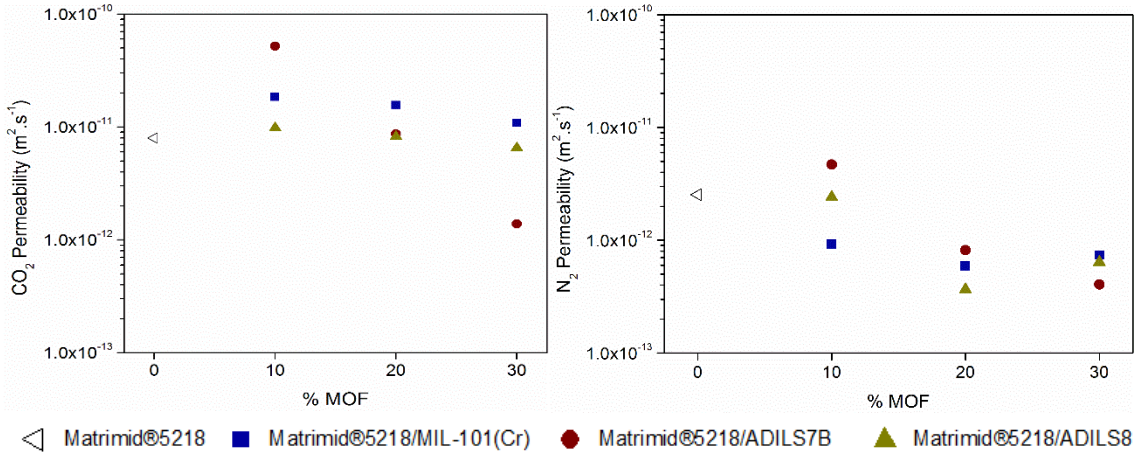

Figure 3.24 – CO_2 (left) and N_2 (right) permeability results of Matrimid®5218, Matrimid®5218/MIL-101(Cr), Matrimid®5218/ADILS7B and Matrimid®5218/ADILS8 membranes at 30ºC.

Also, as described in **section 2.2.9**, with the permeation data of both pure gases, CO_2/N_2 ideal selectivity was determined for all tested membranes. The obtained values are represented in **Table 3.5**.

Table 3.5 – CO_2/N_2 ideal selectivies of Matrimid®5218, Matrimid®5218/MIL-101(Cr), Matrimid®5218/ADILS7B and Matrimid®5218/ADILS8

Filler (wt%, loading)	Ideal selectivity ($\alpha CO_2/N_2$)		
	MIL-101(Cr)	ADILS7B	ADILS8
0%	3.16	3.16	3.16
10%	5.40	11.11	4.08
20%	26.40	10.66	22.54
30%	14.76	3.42	10.23

Through the analysis of **Figure 3.24** it is possible to observe that all the prepared membranes are more permeable to CO_2 than N_2. This phenomenon is explained by the solution-diffusion mechanism that describes the gas transport in nonporous membranes. According to this mechanism the permeability (P) is dependent on the diffusivity (D) and solubility (S) coefficient of the used gas (**Equation 3.1**). [36]

$$P = D \times S \qquad \textbf{(Eq 3.1)}$$

Therefore, since the N_2 Lennard Jones molecular diameter (3.46Å) is a little lower than CO_2 (3.94Å)[66] it is expectable that $D_{N2} > D_{CO2}$, which means that N_2 permeability is mainly controlled by its diffusion in the membranes when compared to CO_2. However, CO_2 molecules are more soluble in the membranes when compared to the N_2 molecules ($S_{CO2} >> S_{N2}$), which explains the higher CO_2 permeability over N_2. Matrimid®5218 membrane showed a high CO_2

permeability ($7.99x10^{-12}$ $m^2.s^{-1}$) over N_2 ($2.53x10^{-12}$ $m^2.s^{-1}$), and these values are in accordance with previous reported works.[44,57,80]

For Matrimid®5218/MIL-101(Cr) mixed matrix membranes, a CO_2 permeability higher than the Matrimid membrane is observed for all MOF incorporation percentages. However, with the increase of MOF loading in the polymeric matrix, a decrease in CO_2 permeability occurs, being the highest value achieved for the Matrimid®5218+10%MIL-101(Cr) membrane ($1.84x10^{-11}$ $m^2.s^{-1}$). This decrease can be related with the rigidification of the polymer chains upon the addition of the MOF, that not allows their normal mobility leading to a decrease in permeability[48], which is in accordance with the puncture tests measurements (**section 3.2.4**) where a raise in the rigidness of the membranes with the increase of MOF loading in the polymeric matrix was verified. Moreover, the higher CO_2 permeability in MIL-101(Cr) membranes compared to Matrimid®5218 membrane is related with the high affinity that this MOF has with CO_2.[57]

Regarding, Matrimid®5218/ADILS7B membranes it is verified an increase in CO_2 permeability compared with the Matrimid®5218/MIL-101(Cr) membranes, for the Matrimid®5218+10%ADILS7B. Regarding CO_2/N_2 ideal selectivity, a decrease was observed with an increase of ADILS7B loading, which may be related with the presence of cavities (shown in SEM images – **section 3.2.1**).

In the case of Matrimid®5218/ADILS8 membranes, for the all incorporation percentages of the IL@MOF, lower CO_2 permeabilities than MIL-101(Cr) membranes were observed.

Finally, in order to evaluate if the prepared membranes performance represent some enhancement relatively to the ones already reported in the literature, the CO_2 permeability and CO_2/N_2 ideal selectivity obtained data for Matrimid®5218, Matrimid®5218/MIL-101(Cr), Matrimid®5218/ADILS7B and Matrimid®5218/ADILS8 membranes was represented with the Robeson upper bound (**Figure 3.25**).[47]

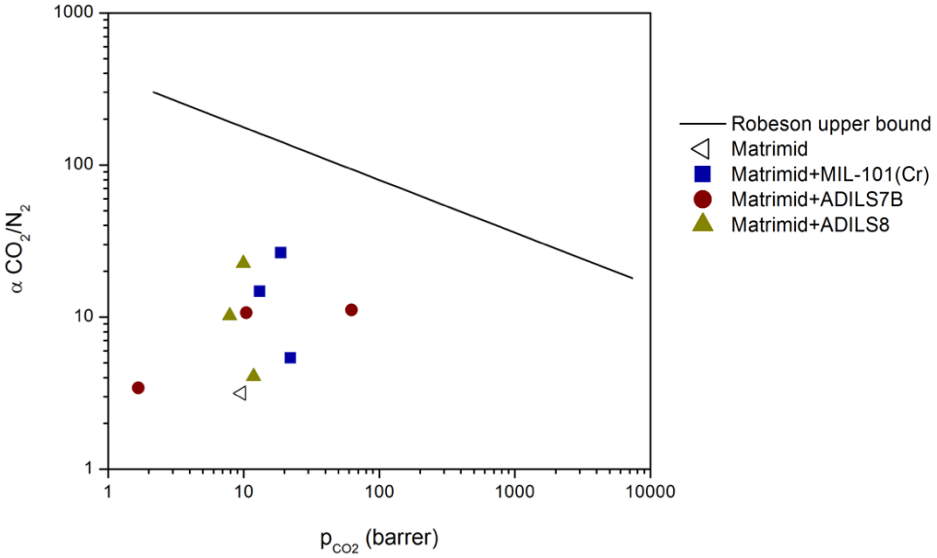

Figure 3.25 – CO_2/N_2 ideal selectivity as a function of CO_2 permeability.

In **Figure 3.25** it is possible to observe that all the values are below the Robeson upper bound, which means that any of the prepared membranes achieve an ideal relation between the CO_2 permeability and CO_2/N_2 ideal selectivity. Although, is possible to observe an increase in CO_2 permeability when compared to the Matrimid®5218 and depending on the IL@MOF or MOF degree of incorporation, an increase in the ideal selectivity was obtained.

4. Conclusion

The aim of this thesis was the development of new mixed matrix membranes (MMMs) with metal-organic frameworks (MOFs) supporting ionic liquids for CO_2 capture from post-combustion flue gas streams. The MOF MIL-101(Cr) and two new IL@MOF systems, [PMIM][Br]@MIL-101(Cr) (ADILS7A and ADILS7B) and [BMIM][Br]@MIL-101(Cr) (ADILS8) were studied.

Due to the novelty of the IL@MOF systems, adsorption equilibria studies were carried out. The results from the N_2 adsorption isotherm at 77K showed that both ADILS7A and ADILS7B did not possess any superficial area and for that reason only ADILS8 and MIL-101(Cr) adsorption equilibria were studied.

From the adsorption equilibria, it was possible to verify that CO_2 was more adsorbed than N_2, due to its high affinity with both adsorbents. Also, MIL-101(Cr) adsorbed higher quantities of both pure gases than ADILS8, suggesting the existence of a high pore filling by [BMIM][Br] in MIL-101(Cr) porous structure. Furthermore, MIL-101(Cr) also showed a high CO_2/N_2 ideal selectivity than ADILS8 indicating that the incorporation of the ionic liquid in the MOF porous structure did not enhanced the CO_2/N_2 ideal selectivity and CO_2 adsorption capacity.

The study of the membranes, Matrimid®5218, Matrimid®5218/MIL-101(Cr), Matrimid®5218/ADILS7B and Matrimid®5218/ADILS8 allowed to evaluate their performance for the separation of CO_2.

The incorporation of MOF and IL@MOF systems in the polymeric matrix produced dense membranes, with a good interaction between the polymer and the MOF or IL@MOF. Also, from the Energy-Dispersive X-ray Spectroscopy (EDS) analysis to Matrimid®5218/MIL-101(Cr) and Matrimid®5218/ADILS8 membranes a good dispersion of the filler in the membranes surface was verified.

From the puncture tests, it was observed that the incorporation of MIL-101(Cr) in the polymeric matrix decreased the tensile strength of the MMMs, turning them less resistant and flexible, while with the incorporation of the ionic liquids in the porous structure of MIL-101(Cr) an increase in the tensile strength occurred. Thus, it can be concluded that the addition of ionic liquids is advantageous for the mechanical properties of the membranes turning them more resistant and flexible.

The results of the contact angles measurements showed that the incorporation of MOF and IL@MOF increased the hydrophilicity of the MMMs. This increase is due to the high affinity of the MOF and both ionic liquids with water. Furthermore, thermogravimetric analysis showed

that all membranes were stable up to 300ºC, indicating that all membranes can withstand the temperatures of post-combustion gas flues streams that normally are between 100-200ºC.

From the gas permeation results, it was observed that all membranes are more permeable to CO_2 than N_2. Also, with the incorporation of MIL-101(Cr) in the polymeric matrix higher CO_2 permeabilities are observed, being the Matrimid+10%MIL-101(Cr) the membrane with the highest CO_2 permeability value. Regarding the IL@MOF systems, with the addition of ADILS7B ([PMIM][Br]@MIL-101(Cr)) in the polymeric matrix a decrease in CO_2/N_2 ideal selectivity was observed. This decrease can be related with the existence of cavities in the surface and cross section of the membranes. In the case of ADILS8 ([BMIM][Br]@MIL-101(Cr)) membranes a decrease in CO_2 permeability when compared to MIL-101(Cr) membranes was observed.

In conclusion, the incorporation of both MOF and IL@MOF systems in the polymeric matrix is advantageous for the membranes performance in CO_2/N_2 gas separation.

5. Future Work

From all the results obtained in this thesis relatively to both adsorption equilibria and membrane gas permeation using MIL-101(Cr) and the newly IL@MOF ADILS7B and ADILS8 samples, some suggestions to improve this study and possible for future work are presented:

1. Study the effect of different ionic liquid concentrations incorporated in the MOF.
2. Measure adsorption/desorption equilibria of the studied materials at higher temperatures, such as 50ºC and 80ºC.
3. Study the effect of the temperature in the membranes permeability by performing gas permeation studies at higher temperatures.
4. Carry out gas permeation studies on the membranes using binary gas mixtures, namely CO_2/N_2 that mimic the composition, temperature and pressure of a flue gas stream.

6. References

1. Li, J. R. *et al.* Carbon dioxide capture-related gas adsorption and separation in metal-organic frameworks. *Coord. Chem. Rev.* **255,** 1791–1823 (2011)
2. D.Figueiroa, J., Fout, T., Plasynski, S., Mcilvried, H. & Srivastava, R. D. Advances in CO_2 capture technology — The U. S. Department of Energy's Carbon Sequestration Program. *Int. J. Greenh. Gas Control* **2,** 9–20 (2008)
3. Wennersten, R., Sun, Q. & Li, H. The future potential for Carbon Capture and Storage in climate change mitigation e an overview from perspectives of technology, economy and risk. *J. Clean. Prod.* **103,** 724–736 (2015)
4. Fossil Fuels by Environmental and Energy Study Institute at <http://www.eesi.org/topics/fossil-fuels/description> (Access date: 23-07-2017)
5. Wu, X., Yu, Y., Qin, Z. & Zhang, Z. The Advances of Post-Combustion CO_2 Capture with Chemical Solvents: Review and Guidelines. *Energy Procedia* **63,** 1339–1346 (2014)
6. Climate Changes: Vital Signs of the Planet at <https://climate.nasa.gov/effects/> (Access date: 23-07-2017)
7. Abdul, F. *et al.* Pollution to solution: Capture and sequestration of carbon dioxide (CO_2) and its utilization as a renewable energy source for a sustainable future. *Renew. Sustain. Energy Rev.* **71,** 112–126 (2017)
8. Global Climate Change: Vital signs of the planet (NASA) at <https://climate.nasa.gov/vital-signs/carbon-dioxide/> (Access date: 29-07-2017)
9. The science of carbon dioxide and climate change at <https://phys.org/news/2017-03-science-carbon-dioxide-climate.html> (Access date: 29-07-2017)
10. International Energy Agency. CO_2 emissions from fuel combustion (2016 Highlights). 166 (2016)
11. Leung, D. Y. C., Caramanna, G. & Maroto-valer, M. M. An overview of current status of carbon dioxide capture and storage technologies. *Renew. Sustain. Energy Rev.* **39,** 426–443 (2014)
12. Paris Agreement 2015 at <https://ec.europa.eu/clima/policies/international/negotiations/paris_en> (Access date: 30-07-2017)
13. Sreedhar, I., Nahar, T., Venugopal, A. & Srinivas, B. Carbon capture by absorption – Path covered and ahead. *Renew. Sustain. Energy Rev.* **76,** 1080–1107 (2017)
14. Deanna M. D'Alessandro, Berend Smith, J. R. L. Carbon dioxide capture: Prospects for new materials. *Angew. Chemie* **49,** 6058–6082 (2010)
15. Wang, M., Lawal, A., Stephenson, P., Sidders, J. & Ramshaw, C. Post-combustion CO_2 capture with chemical absorption: A state-of-the-art review. *Chem. Eng. Res. Des.* **89,** 1609–1624 (2011)
16. Fact Sheet: Transport of CO_2, at

<https://hub.globalccsinstitute.com/sites/default/files/publications/25906/transport-co2.pdf> (access date: 02-08-2017). 2 (2012)

17. Coninck, H. De & Benson, S. M. Carbon Dioxide Capture and Storage : Issues and Prospects. *Annu. Rev. Environ. Resour.* **39,** 243–270 (2014)
18. Kanniche, M. *et al.* Pre-combustion, post-combustion and oxy-combustion in thermal power plant for CO_2 capture. *Appl. Therm. Eng.* **30,** 53–62 (2015)
19. Folger, P. *Carbon Capture : A Technology Assessment - report R41325*. (2010)
20. S.N. Pandey, Sanjeev Kumar Gupta, Abhishek Tomar, A. K. Post combustion carbon capture technology - Paper No.56. in *National Conference on Eco friendly Manufacturing for Sustainable Development* (ed. GLA University) 1–8 (GLA University, 2010)
21. Bert Metz, Ogunlade Davidson, Heleen de Coninck, Manuela Loos, L. M. *IPCC special report on carbon dioxide capture and storage*. (Cambrigde University Press, 2015)
22. Khutia, A. & Janiak, C. Programming MIL-101Cr for selective and enhanced CO_2 adsorption at low pressure by postsynthetic amine functionalization. *Dalt. Trans.* **43,** 1338–1347 (2014)
23. F. Rouquerol, J.Rouquerol, K. S. *Adsorption by powders & porous solids (first edition)*. (Academic Press, 1999)
24. Douglas M.Ruthven. *Principles of Adsorption and Adsorption Processes (first edition)*. (John Willey & Sons, 1984)
25. Jürgun Keller, R. S. *Gas adsorption equilibria - Experimental methods and adsorption isotherms (first edition)*. (Springer, 2005)
26. Dabrowsky, A. Adsorption - from theory to practice. *Adv. Colloid Interface Sci.* **93,** 135–224 (2001)
27. Thommes, M. *et al.* Physisorption of gases, with special reference to the evaluation of surface area and pore size distribution (IUPAC Technical Report). *Pure Appl. Chem* **87,** 1–19 (2015)
28. Ribeiro, R. P. P. L., Silva, R. J. S., Esteves, I. A. A. C. & Mota, J. P. B. Development, Construction, and Operation of a Multisample Volumetric Apparatus for the Study of Gas Adsorption Equilibrium. *J. Chem. Educ.* **92,** 757–761 (2015)
29. Camacho, B. C. R., Ribeiro, R. P. P. L., Esteves, I. A. A. C. & Mota, J. P. B. Adsorption equilibrium of carbon dioxide and nitrogen on the MIL-53 (Al) metal organic framework. *Sep. Purif. Technol.* **141,** 150–159 (2015)
30. Do, D. D. *Adsorption analysis: Equilibria and kinetics (first edition)*. **2,** (Imperial College Press, 1998)
31. Munusamy, K. *et al.* Sorption of carbon dioxide, methane, nitrogen and carbon monoxide on MIL-101(Cr): Volumetric measurements and dynamic adsorption studies. *Chem. Eng. J.* **195–196,** 359–368 (2012)
32. M.G. Plaza, S. García, F. Rubiera, J.J. Pis, C. P. Post-combustion CO_2 capture with a commercial activated carbon: comparison of different regeneration strategies. *Chem. Eng. J.* **163,** 1–28 (2010)

33. Riboldi, L., Bolland, O., Ngoy, J. M. & Wagner, N. Full-plant analysis of a PSA CO_2 capture unit integrated in coal- fired power plants: post- and pre-combustion scenarios. *Energy Procedia* **63,** 2289–2304 (2014)
34. Esteves, I. A. A. C. Gas separation processes by integrated adsorption and permeation technologies (PhD Thesis). (2005)
35. Aroon, M. A. & Ismail, A. F. Performance studies of mixed matrix membranes for gas separation: A review. *Sep. Purif. Technol.* **75,** 229–242 (2010)
36. Mulder, M. *Basic principles of membrane technology (second edition)*. (Kluwer Academic Publishers, 2003)
37. Wang, S. *et al.* Advances in high permeability polymer-based membrane materials for CO_2 separations. *Energy Environ. Sci.* **9,** 1863–1890 (2016)
38. Jeazet, H. B. T. *et al.* Increased Selectivity in CO_2/CH_4 Separation with Mixed-Matrix Membranes of Polysulfone and Mixed-MOFs MIL-101(Cr) and ZIF-8. *Eur. J. Inorg. Chem.* 4363–4367 (2016)
39. Goh, P. S., Ismail, A. F., Sanip, S. M., Ng, B. C. & Aziz, M. Recent advances of inorganic fillers in mixed matrix membrane for gas separation. **81,** 243–264 (2011)
40. Yang, T. & Chung, T. High performance ZIF-8/PBI nano-composite membranes for high temperature hydrogen separation consisting of carbon monoxide and water vapor. *Int. J. Hydrogen Energy* **38,** 229–239 (2013)
41. Li, W., Zhang, Y., Li, Q. & Zhang, G. Metal-organic framework composite membranes : Synthesis and separation applications. *Chem. Eng. Sci.* **135,** 232–257 (2015)
42. Rezakazemi, M., Ebadi Amooghin, A., Montazer-Rahmati, M. M., Ismail, A. F. & Matsuura, T. State-of-the-art membrane based CO_2 separation using mixed matrix membranes (MMMs): An overview on current status and future directions. *Prog. Polym. Sci.* **39,** 817–861 (2014)
43. Adatoz, E., Avci, A. K. & Keskin, S. Opportunities and challenges of MOF-based membranes in gas separations. *Sep. Purif. Technol.* **152,** 207–237 (2015)
44. Perez, E. V, Jr, K. J. B., Ferraris, J. P. & Musselman, I. H. Mixed-matrix membranes containing MOF-5 for gas separations. **328,** 165–173 (2009)
45. Shahid, S. *et al.* MOF-mixed matrix membranes: Precise dispersion of MOF particles with better compatibility via a particle fusion approach for enhanced gas separation properties. *J. Memb. Sci.* **492,** 21–31 (2015)
46. Robeson, L. M. Correlation of separation factor versus permeability for polymeric membranes. *J. Memb. Sci.* **62,** 165–185 (1991)
47. Robeson, L. M. The upper bound revisited. *Jounal Membr. Sci.* **320,** 390–400 (2008)
48. Zornoza, B., Tellez, C., Coronas, J., Gascon, J. & Kapteijn, F. Metal organic framework based mixed matrix membranes: An increasingly important field of research with a large application potential. *Microporous Mesoporous Mater.* **166,** 67–78 (2013)
49. Dorosti, F., Omidkhah, M. & Abedini, R. Fabrication and characterization of Matrimid/MIL-53 mixed matrix membrane for CO_2/CH_4 separation. *Chem. Eng. Res. Des.* **92,** 2439–

2448 (2014)

50. Khdhayyer, M. R. *et al.* Mixed matrix membranes based on UiO-66 MOFs in the polymer of intrinsic microporosity PIM-1. *Sep. Purif. Technol.* **173,** 304–313 (2017)
51. Monteiro, B. *et al.* Membranes with a low loading of Metal- Organic Framework-Supported Ionic Liquids for CO_2/N_2 separation in CO_2 capture. *Energy Technol.* **5,** 0–5 (2017)
52. Fujie, K. & Kitagawa, H. Ionic liquid transported into metal – organic frameworks. *Coord. Chem. Rev.* **307,** 382–390 (2016)
53. C.Tomé, L. Development of new membranes based on ionic liquid materials for gas separation (phD Thesis). (2014)
54. C.Tomé, L. & Marrucho, I. M. Chem Soc Rev. *Chem. Soc. Rev.* **45,** 2785–2824 (2016)
55. Tin, P. S. *et al.* Effects of cross-linking modification on gas separation performance of Matrimid membranes. *J. Memb. Sci.* **225,** 77–90 (2003)
56. Hunstman Advanced Materials Inc. Matrimid ® 5218 / Matrimid ® 9725 (Technical Datasheet). 1–7 (2015)
57. Naseri, M., Mousavi, S. F., Mohammadi, T. & Bakhtiari, O. Synthesis and gas transport performance of MIL-101/Matrimid mixed matrix membranes. *J. Ind. Eng. Chem.* **29,** 249–256 (2015)
58. Liu, Q. *et al.* Adsorption of Carbon Dioxide by MIL-101(Cr): Regeneration Conditions. *Sci. Rep.* **2,** 1–6 (2013)
59. Zhou, Z. *et al.* A novel bimetallic MIL-101 (Cr, Mg) with high CO_2 adsorption capacity and CO_2/N_2 selectivity. *Chem. Eng. Sci.* **147,** 109–117 (2016)
60. Cho, C., Phuong, T., Pham, T., Jeon, Y. & Vijayaraghavan, K. Toxicity of imidazolium salt with anion bromide to a phytoplankton Selenastrum capricornutum: Effect of alkyl-chain length. *Chemosphere* **69,** 1003–1007 (2007)
61. Sadeghi, R. & Shekaari, H. Volumetric and Isentropic Compressibility Behavior of Ionic Liquid, 1-Propyl-3-Methylimidazolium Bromide in Acetonitrile, Dimethylformamide,. *Int. J. Thermophys.* **30,** 1491–1509 (2009)
62. Eyupoglu, V. & Polat, E. Fluid Phase Equilibria Evaluation of Cd (II) transport with imidazolium bromides bearing butyl and isobutyl groups as extractants from acidic iodide solutions by liquid – liquid solvent extraction. *Fluid Phase Equilib.* **394,** 46–60 (2015)
63. Serre, C., Millange, F. & Fe, G. A Chromium Terephthalate – Based Solid with Unusually Large Pore Volumes and Surface Area. *Science.* **309,** 2040–2042 (2005)
64. Parhnam, E. R. & Russel E. Morris. 1-alkyl-3-methylimidazolium bromide ionic liquids in the ionothermal synthesis of aluminium phosphate molecular sieves. *Chem. Mater.* **18,** 4882–4887 (2006)
65. National Institute of Standards and Technology - NIST at <http://webbook.nist.gov/chemistry/> (Access date: 28-07-2017)
66. E.L.Cussler. *Diffusion: Mass Transfer in Fluid Systems (third edition)*. (Cambrigde University Press, 1997)
67. Ye, S. *et al.* Post-combustion CO_2 capture with the HKUST-1 and MIL-101(Cr) metal-

organic frameworks: Adsorption, separation and regeneration investigations. *Microporous Mesoporous Mater.* **179,** 191–197 (2013)

68. Peluso, A., Gargiulo, N., Aprea, P., Pepe, F. & Caputo, D. Modeling Hydrogen Sulfide Adsorption on Chromium-Based MIL-101 Metal Organic Framework. *Sci. Adv. Mater.* **6,** 1–7 (2014).
69. Chowdhury, P., Bikkina, C. & Gumma, S. Gas Adsorption Properties of the Chromium-Based Metal Organic Framework MIL-101. *J. Phys. Chem. C* **113,** 6616–6621 (2009)
70. Khan, N. A., Hasan, Z. & Jhung, S. H. Ionic liquid@MIL-101 prepared via the ship-in-bottle technique: Remarkable adsorbents for the removal of benzothiophene from liquid fuel. *Chem. Commun.* **52,** 2561–2564 (2016)
71. Paulechka, Y. U. Thermodynamic properties of 1-alkyl-3-methylimidazolium bromide ionic liquids. *Jounal Chem. Thermodyn.* **39,** 158–166 (2007)
72. Siedlecka, E. M., Czerwicka, M., Stolte, S. & Stepnowski, P. Stability of Ionic Liquids in Application Conditions. *Curr. Org. Chem.* **15,** 1974–1991 (2011)
73. Sun, X., Xia, Q., Zhao, Z., Li, Y. & Li, Z. Synthesis and adsorption performance of MIL-101 (Cr)/ graphite oxide composites with high capacities of n-hexane. *Chem. Eng. J.* **239,** 226–232 (2014)
74. Anbia, M. Enhancement of CO_2 adsorption on nanoporous chromium terephthalate (MIL-101) by amine modification. *J. Nat. Gas Chem.* **21,** 339–343 (2012)
75. Chowdhury, P., Mekala, S., Dreisbach, F. & Gumma, S. Adsorption of CO, CO_2 and CH_4 on Cu-BTC and MIL-101 metal organic frameworks: Effect of open metal sites and adsorbate polarity. *Microporous Mesoporous Mater.* **152,** 246–252 (2012)
76. Ren, J., Musyoka, N. M. & Langmi, H. W. Fabrication of core e shell MIL-101(Cr)@ UiO-66 (Zr) nanocrystals for hydrogen storage. *Int. J. Hydrogen Energy* **39,** 14912–14917 (2014)
77. Ardelean, O. *et al.* Volumetric hydrogen adsorption capacity of densified MIL-101 monoliths. *Int. J. Hydrogen Energy* **38,** 7046–7055 (2013)
78. Zhang, Y. *et al.* Adsorption Equilibrium of N_2, CH_4 and CO_2 on MIL-101. *J. Chem. Eng. data* (2015)
79. Li, P., Chen, J., Feng, W. & Wang, X. Adsorption separation of CO_2 and N_2 on MIL-101 metal-organic framework and activated carbon. *J. Iran. Chem. Soc.* **11,** 741–749 (2014)
80. Zhang, Y., Musselman, I. H., Ferraris, J. P. & Jr, K. J. B. Gas permeability properties of Matrimid® membranes containing the metal-organic framework Cu – BPY – HFS. *Jounal Membr. Sci.* **313,** 170–181 (2008)
81. Online, V. A., Ge, L., Zhou, W., Rudolph, V. & Zhu, Z. Mixed matrix membranes incorporated with size-reduced Cu-BTC for improved gas separation†. *J. Mater. Chem. A* **1,** 6350–6358 (2013)
82. Ying, L. & Shung, T. Beta-Cyclodextrin containing Matrimid® sub-nanocomposite membranesmembranes for pervaporation application. *Jounal Membr. Sci.* **327,** 216–225 (2009)

83. Chung, T., Fen, W. & Liu, Y. Enhanced Matrimid membranes for pervaporation by homogenous blends with polybenzimidazole (PBI). *Jounal Membr. Sci.* **271,** 221–231 (2006)
84. Sorribas, S., Gorgojo, P. & Livingston, A. G. High Flux Thin Film Nanocomposite Membranes Based on Metal − Organic Frameworks for Organic Solvent Nano filtration. *J. Am. Chem. Soc.* **135,** 15201–15208 (2013)
85. Smallwood, I. M. *Handbook of organic solvent properties (first edition)*. (Jonh Wiley & Sons, 1996)
86. Barreto, N. Desenvolvimento de Membranas para Separação de Gases contendo MOFs (Metal Organic Frameworks) (Master Thesis). RUN: http://hdl.handle.net/10362/7729. (2012)
87. Nabais, R. Preparação e caracterização de membranas de matriz mista para separação de CO2 (Master Thesis). RUN: http://hdl.handle.net/10362/19710. (2016)
88. Hao Li, Linghan Tuo, Kai Yang, Hae-Kwon Jeong, Yan Dai, Gaohong He, W. Z. Simultaneous enhancement of mechanical properties and CO_2 selectivity of ZIF-8 mixed matrix membranes: Interfacial toughening effect of ionic liquid. *J. Memb. Sci.* **511,** 130–143 (2016)
89. Samanta, A., Zhao, A., Shimizu, G. K. H., Sarkar, P. & Gupta, R. Post-Combustion CO_2 Capture Using Solid Sorbents : A Review. *Ind. Eng. Chem. Res.* **51,** 1438–1463 (2012)
90. Venna, S. R. *et al.* Fabrication of MMMs with improved gas separation properties using externally-functionalized MOF particles †. *J. Mater. Chem. A* **3,** 5014–5022 (2015)
91. Rubotherm. *Fact Sheet: ISOSORP – The new sorption suspension balance*. (2016)

7. Appendix

7.1 MOF and IL@MOF synthesis

7.1.1 Materials

All the reagents were used as received: 3-propyl-1methylimidazolium bromide (1-methylimidazole, Sigma-Aldrich, 99%; 1-bromopropane, Aldrich, 99%), 3-butyl-1methylimidazolium bromide (1-methylimidazole, Sigma-Aldrich, 99%; 1-bromobutane, Sigma-Aldrich, 99%) and the chromium MOF [MIL-101(Cr)] (chromium(III) nitrate nonahydrate, Aldrich, 99%; terephthalic acid, Aldrich, 98%).

7.1.2 MOF and IL@MOF synthesis

MIL-101(Cr)

The porous MOF was synthesized by following the original method described by Férey and co-workers. [63] A mixture of chromium(III) nitrate (2 mmol), benzene-1,4-dicarboxylic acid (2 mmol) and hydrofluoric acid (100 µL) in 10 mL of H_2O was stirred to obtain a homogeneous suspension at room temperature, transferred to an autoclave and heated at 493 K for 9 h in an electric oven. After slow cooling (inside the oven), the resultant material was isolated by filtration and purified through a double DMF treatment followed by a double ethanol treatment.

1-Propyl-3-Methylimidazolium Bromide ([PMIM][Br])

The ionic liquid was prepared according to literature. [64] Briefly, 1-Methylimidazole (17.5 mL, 220 mmol) was mixed with 1-Bromopropane (35.5 mL, 390 mmol), under constant stirring and refluxed at 70 °C for 5 hours. Afterwards, the final product was washed 5 times with ethyl acetate and excess ethyl bromide was removed by rotary evaporation. The remnant was dried under vacuum at 50 °C for 10 h to give a colorless oil.

[PMIM][Br]@MIL-101(Cr) – ADILS7A and ADILS7B

Direct Contact Method (DM) – 2 g of porous MIL-101(Cr) were added to a 10mL solution [PMIM][Br] / Dichloromethane (6:4) and stirred for 30 mins (ADILS7A) and 45 mins (ADILS7B). The resultant material was isolated by centrifugation and washed 3 times with dichloromethane.

[BMIM][Br]@MIL-101(Cr) – ADILS8

Ship in the Bottle Method (SIP) – 17 g of 1-Methylimidazole were mixed with 2 g of MIL-101(Cr) and stirred at room temperature for 15h. Afterwards, 28 g of 1-Bromobutane were added and the mixture was stirred for 24h at room temperature. The resultant material was isolated by

filtration and transferred to an ethanol hot bath at 70 ºC for 24h. A new filtration followed to isolate the final material and purification was done by washing it 3 times with ethanol.

7.2 Powder X-ray Diffraction and FTIR analyses

Powder X-ray diffraction analyses were collected at ambient temperature in Bragg-Brentano para-focusing geometry using Rigaku Smartlab diffractometer, equipped with D/teX Ultra 250 detector, in Cu K-alpha radiation (Ka1 wavelength 1.54059 ang), 45 kV, 200 mA, in continuous mode, step 0.01º, speed 15º/min, in the range $1 \leq 2\theta \leq 50^{\circ}$ (**Figure 7.1**).

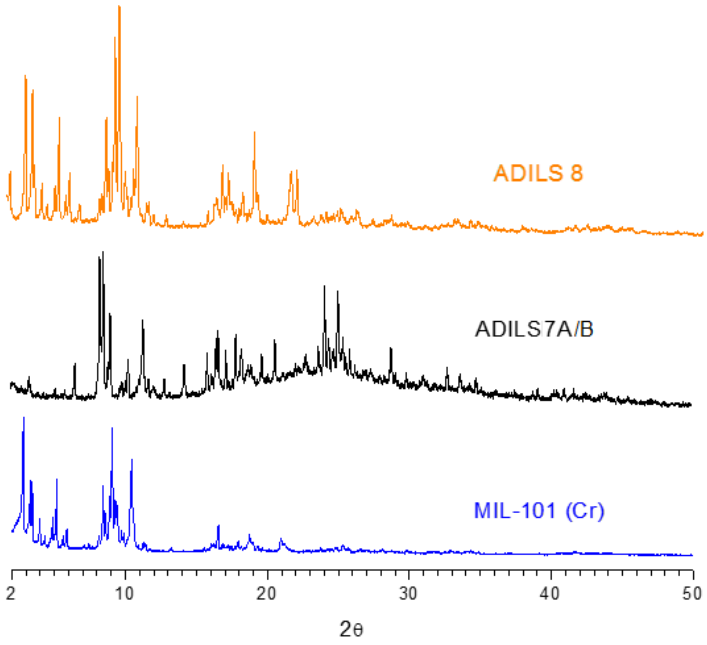

Figure 7.1 – X-ray powder difraction to MIL-101(Cr), ADILS7A/B and ADILS8.

Infrared absorption spectra were recorded on a PerkinElmer spectrum BX FTIR spectrometer (**Figure 7.2**)

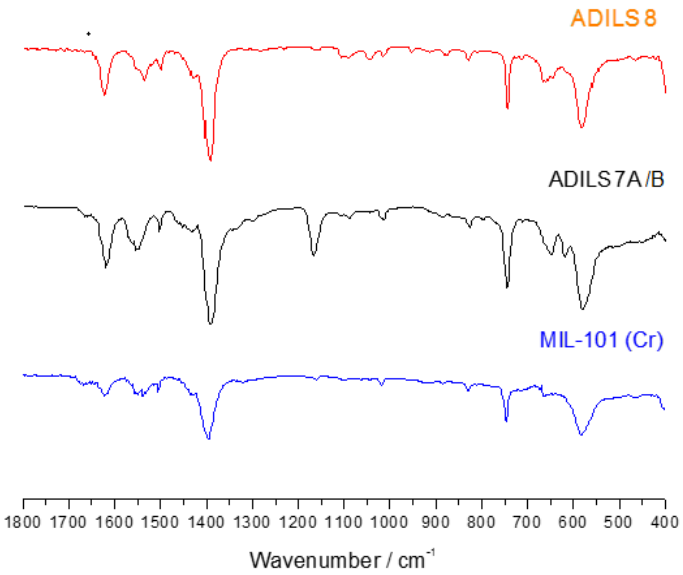

Figure 7.2 – FTIR spectrum of MIL-101(Cr), ADILS7A/B and ADILS8.

7.3 Adsorption/desorption equilibria

Table 7.1 – N_2 adsorption/desorption equilibria on MIL-101(Cr) at 30ºC

Point	Temperature (ºC)	Pressure (bar)	Weighted Mass (g)	ρ (Kg.m^{-3})	qnet (g/g)	qex (g/g)	qt (g/g)	qnet (mol/Kg)	qex (mol/Kg)	qt (mol/Kg)
0	30.09	0.000	6.57972	0.0000	0.000000	0.000000	0.000000	0.000000	0.000000	0.000000
1	30.06	0.4054	6.57998	0.4505	0.002477	0.002736	0.003198	0.088435	0.097664	0.114164
2	30.04	0.7325	6.57992	0.8141	0.003402	0.003869	0.004704	0.121440	0.138117	0.167935
3	30.07	2.319	6.57957	2.5773	0.007649	0.009128	0.011772	0.273096	0.325894	0.420291
4	30.05	4.744	6.57879	5.2757	0.013177	0.016204	0.021617	0.470443	0.578521	0.771749
5	30.03	7.253	6.57801	8.0680	0.019005	0.023635	0.031912	0.678517	0.843798	1.139298
6	30.03	10.023	6.57692	11.155	0.024542	0.030943	0.042386	0.876177	1.104697	1.513263
7	30.03	6.002	6.57854	6.676	0.016662	0.020493	0.027342	0.594862	0.731625	0.976142
8	30.01	3.520	6.57923	3.914	0.010573	0.012819	0.016835	0.377474	0.457660	0.601022
9	30.08	1.674	6.57963	1.8604	0.005594	0.006662	0.008571	0.199730	0.237842	0.305982

Table 7.2 – N_2 adsorption/desorption equilibria on ADILS8 at 30ºC

Point	Temperature (ºC)	Pressure (bar)	Weighted Mass (g)	ρ (Kg/m^3)	qnet (g/g)	qex (g/g)	qt (g/g)	qnet (mol/Kg)	qex (mol/Kg)	qt (mol/Kg)
0	30.09	0.000	5.45505	0.0000	0.000000	0.000000	0.000000	0.000000	0.000000	0.000000
1	30.06	0.4054	5.45485	0.4505	0.001027	0.001298	0.001663	0.036663	0.046328	0.059375
2	30.04	0.7325	5.45463	0.8141	0.001294	0.001783	0.002443	0.046181	0.063646	0.087223
3	30.07	2.319	5.45377	2.5773	0.004572	0.006120	0.008211	0.163213	0.218504	0.293146
4	30.05	4.744	5.45221	5.2757	0.007248	0.010418	0.014698	0.258760	0.371941	0.524731
5	30.03	7.253	5.45051	8.0680	0.009195	0.014043	0.020587	0.328260	0.501345	0.735003
6	30.03	10.023	5.44863	11.155	0.011341	0.018044	0.027093	0.404897	0.644208	0.967269
7	30.03	6.002	5.45130	6.676	0.007672	0.011684	0.017100	0.273920	0.417142	0.610486
8	30.01	3.520	5.45296	3.914	0.005541	0.007893	0.011069	0.197834	0.281807	0.395166
9	30.08	1.674	5.45415	1.8604	0.003530	0.004648	0.006157	0.126022	0.165934	0.219813

Table 7.3 – CO_2 adsorption/desorption equilibria on MIL-101(Cr) at 30ºC

Point	Temperature (ºC)	Pressure (bar)	Weighted Mass (g)	ρ (Kg/m^3)	qnet (g/g)	qex (g/g)	qt (g/g)	qnet (mol/Kg)	qex (mol/Kg)	qt (mol/Kg)
0	29.87	0.000	6.57956	0.0000	0.000000	0.000000	0.000000	0.000000	0.000000	0.000000
1	30.01	0.410	6.58721	0.7179	0.032787	0.033199	0.033936	0.744993	0.754353	0.771089
2	30.00	0.804	6.59211	1.4085	0.054527	0.055335	0.056780	1.238962	1.257326	1.290159
3	29.99	2.990	6.60817	5.2959	0.130979	0.134018	0.139451	2.976124	3.045173	3.168624
4	30.01	6.898	6.63008	12.4570	0.241228	0.248376	0.261156	5.481215	5.643632	5.934012
5	30.04	7.701	6.63479	13.9620	0.264818	0.272830	0.287153	6.017231	6.199270	6.524733
6	30.02	9.211	6.63918	16.832	0.291504	0.301162	0.318430	6.623576	6.843034	7.235399
7	29.99	5.412	6.62529	9.701	0.213302	0.218868	0.228820	4.846663	4.973145	5.199278
8	30.01	3.657	6.61465	6.498	0.160654	0.164382	0.171049	3.650389	3.735111	3.886584
9	30.00	1.544	6.59798	2.7156	0.082106	0.083664	0.086450	1.865626	1.901032	1.964334

Table 7.4 – CO_2 adsorption/desorption equilibria on ADILS8 at 30ºC

Point	Temperature (ºC)	Pressure (bar)	Weighted Mass (g)	ρ (Kg/m^3)	qnet (g/g)	qex (g/g)	qt (g/g)	qnet (mol/Kg)	qex (mol/Kg)	qt (mol/Kg)
0	29.87	0.000	5.45508	0.0000	0.000000	0.000000	0.000000	0.000000	0.000000	0.000000
1	30.01	0.410	5.45610	0.7179	0.014481	0.014913	0.015495	0.329045	0.338848	0.352081
2	30.00	0.804	5.45681	1.4085	0.025809	0.026655	0.027798	0.586436	0.605668	0.631630
3	29.99	2.990	5.45892	5.2959	0.071473	0.074655	0.078951	1.624013	1.696322	1.793937
4	30.01	6.898	5.46026	12.4570	0.131154	0.138639	0.148744	2.980090	3.150176	3.379786
5	30.04	7.701	5.46053	13.9620	0.143585	0.151975	0.163301	3.262555	3.453190	3.710540
6	30.02	9.211	5.46032	16.832	0.160336	0.170450	0.184104	3.643169	3.872991	4.183241
7	29.99	5.412	5.46031	9.701	0.113612	0.119442	0.127311	2.581515	2.713970	2.892778
8	30.01	3.657	5.45966	6.498	0.086433	0.090338	0.095609	1.963945	2.052667	2.172440
9	30.00	1.544	5.45785	2.7156	0.044335	0.045966	0.048169	1.007374	1.044452	1.094507

7.4 Energy-Dispersive X-ray Spectroscopy (EDS)

In **Figure 7.3** is represented the x-ray mapping images of chromium element (MIL-101(Cr)) on Matrimid®5218/ADILS8 membranes for all percentages of incorporation (10% (w/w), 20%(w/w) and 30%(w/w)).

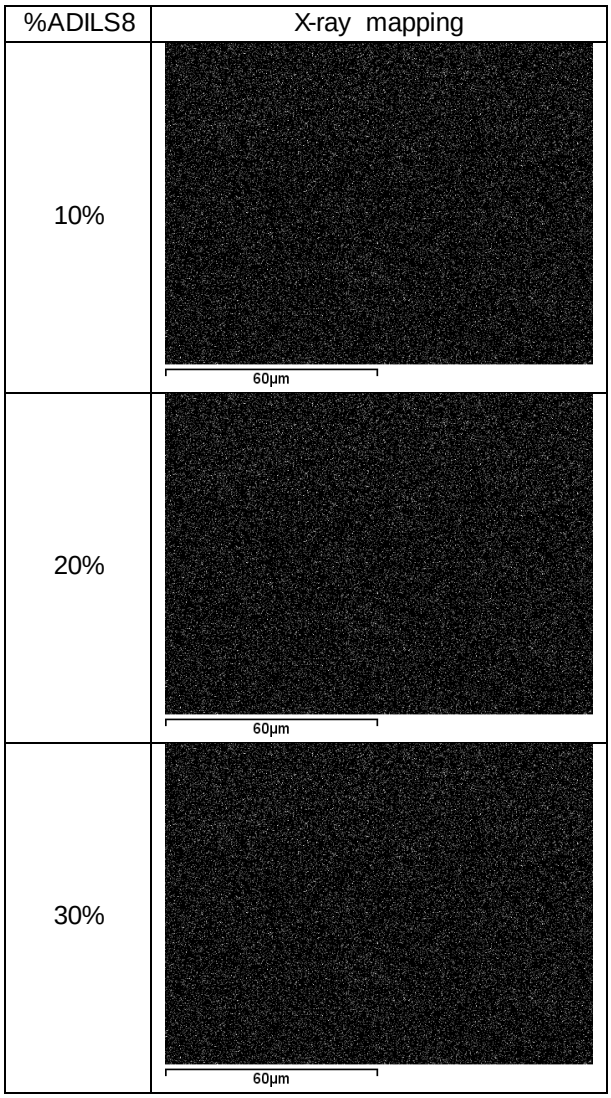

Figure 7.3 – X-ray mapping images of chromium element on Matrimid®5218 /ADILS8 membranes.

7.5 Mechanical Properties

Puncture test results of the Matrimid+10%MIL-101(Cr), Matrimid+20%ADILS7B and Matrimid+30%ADILS8 membranes are represented in **Figure 7.4**, **Figure 7.5** and **Figure 7.6**, respectively.

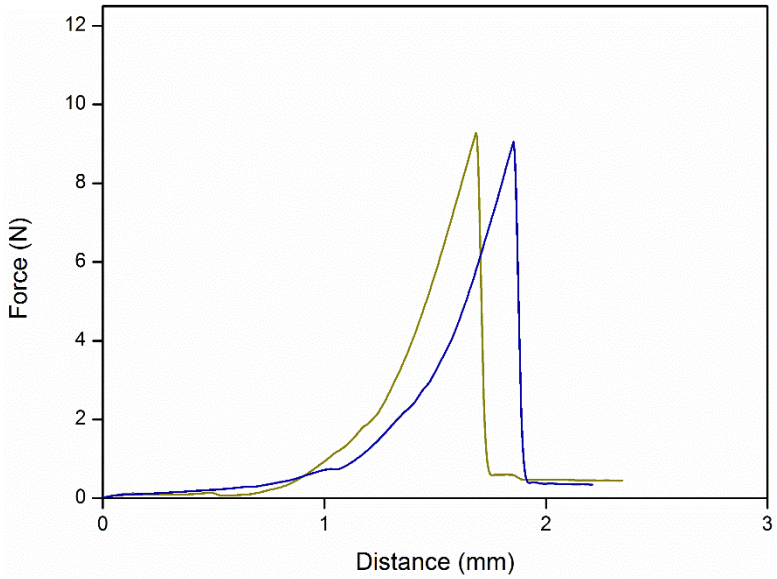

Figure 7.4 – Puncture test results of Matrimid®5218+10%MIL-101(Cr).

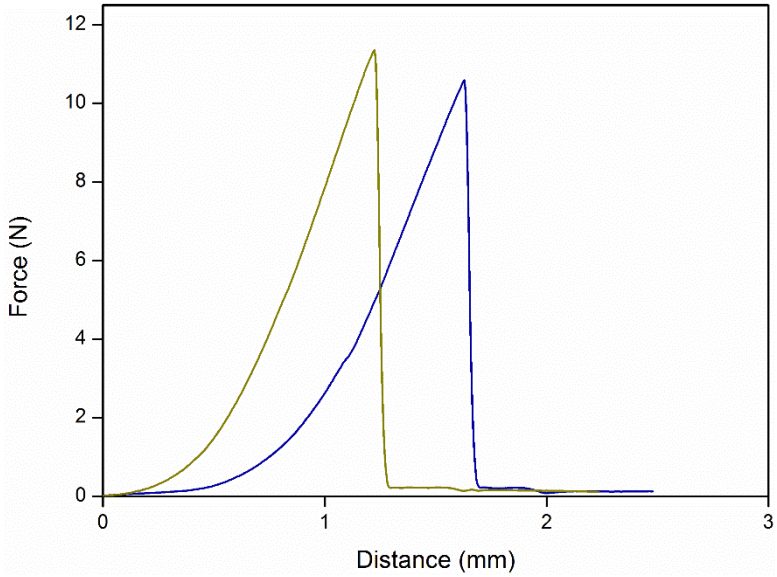

Figure 7.5 – Puncture test results of Matrimid®5218+20%ADILS7B.

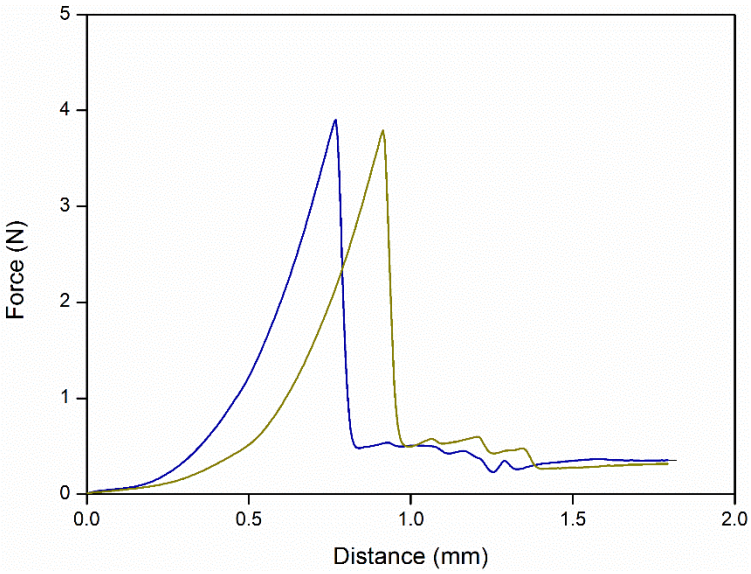

Figure 7.6 – Puncture test results of Matrimid®5218+30%ADILS8.